JV

LEVEL II

AFWAL-TR-81-2036

AD A103639

ISOTHERMAL FLOWFIELD PREDICTIONS OF CONFINED COFLOWING
TURBULENT JETS IN AN AXISYMMETRIC BLUFF-BODY NEAR WAKE

L. KRISHNAMURTHY

UNIVERSITY OF DAYTON RESEARCH INSTITUTE
300 COLLEGE PARK AVENUE
DAYTON, OH 45469

MAY 1981

FINAL REPORT FOR PERIOD 1 JANUARY 1980 – 30 SEPTEMBER 1980

Approved for Public Release, Distribution Unlimited.

DTIC
ELECTE
SEP 2 1981
S D

D

AERO PROPULSION LABORATORY
AIR FORCE WRIGHT AERONAUTICAL LABORATORIES
AIR FORCE SYSTEMS COMMAND
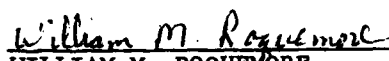WRIGHT PATTERSON AIR FORCE BASE, OHIO 45433

DTIC FILE COPY

81 8 31 226

NOTICE

"When Government drawings, specifications, or other data are used for any purpose other than in connection with a definitely related government procurement operation, the United States Government thereby incurs no responsibility nor any obligation whatsoever; and the fact that the Government may have formulated, furnished, or in any other way supplied the said drawings, specifications, or other data, is not to be regarded by implication or otherwise as in any manner licensing the holder or any other person or corporation, or conveying any rights or permission to manufacture, use, or sell any patented invention that may in any way be related thereto."

This report has been reviewed by the Office of Public Affairs (ASD/PA) and is releasable to the National Technical Information Service (NTIS). At NTIS, it will be available to the general public, including foreign nations.

This technical report has been reviewed and is approved for publication.

WILLIAM M. ROQUEMORE
Project Engineer

ARTHUR V. CHURCHILL
Chief, Fuels Branch

FOR THE COMMANDER

ROBERT D. SHERRILL
Chief, Fuels and Lubrication Division

"If your address has changed, if you wish to be removed from our mailing list, or if the addressee is no longer employed by your organization please notify AFWAL/POSF, W-PAFB, OH 45433 to help us maintain a current mailing list."

Copies of this report should not be returned unless return is required by security considerations, contractual obligations, or notice on a specific document.

REPORT DOCUMENTATION PAGE	READ INSTRUCTIONS BEFORE COMPLETING FORM

1. REPORT NUMBER	2. GOVT ACCESSION NO.	3. RECIPIENT'S CATALOG NUMBER
AFWAL-TR-81-2036	AD-A103 639	

4. TITLE (and Subtitle)	5. TYPE OF REPORT & PERIOD COVERED
Isothermal Flowfield Predictions of Confined Coflowing Turbulent Jets in an Axisymmetric Bluff-Body Near Wake	Final Technical Report. 1 Jan 1980 - 30 Sep 1980
	6. PERFORMING ORG. REPORT NUMBER
	UDR-TR-80-105

7. AUTHOR(s)	8. CONTRACT OR GRANT NUMBER(s)
Dr. L. Krishnamurthy	F33615-77-C-2004

9. PERFORMING ORGANIZATION NAME AND ADDRESS	10. PROGRAM ELEMENT, PROJECT, TASK AREA & WORK UNIT NUMBERS
University of Dayton Research Institute Dayton, OH 45469	2308 S7 06

11. CONTROLLING OFFICE NAME AND ADDRESS	12. REPORT DATE
Air Force Wright-Aeronautical Laboratories Aero Propulsion Laboratory, Wright Patterson AFB Ohio	May 1981
	13. NUMBER OF PAGES
	66

14. MONITORING AGENCY NAME & ADDRESS(if different from Controlling Office)	15. SECURITY CLASS. (of this report)
	Unclassified
	15a. DECLASSIFICATION/DOWNGRADING SCHEDULE

16. DISTRIBUTION STATEMENT (of this Report)

Approved for Public Release, Distribution Unlimited.

17. DISTRIBUTION STATEMENT (of the abstract entered in Block 20, if different from Report)

18. SUPPLEMENTARY NOTES

Funding was provided from Program Element 61102F, WU.2308S706.

19. KEY WORDS (Continue on reverse side if necessary and identify by block number)

Recirculating Flowfields	Confined Turbulent Flows
Isothermal Flows	Coflowing Jets
Bluff-Body Near Wake	Numerical Predictions

20. ABSTRACT (Continue on reverse side if necessary and identify by block number)

Numerical computations are carried out to predict the turbulent flowfields under isothermal conditions in the Aero Propulsion Laboratory (APL) combustor. This combustor consists of an axially symmetrical configuration with a cylindrical bluff body placed inside a duct. Turbulent convection, diffusion and mixing of two coaxial jets - one flowing in the annulus between the duct and the bluff body and the other flowing through a central tube in

DD FORM 1473 EDITION OF 1 NOV 65 IS OBSOLETE

20. ABSTRACT (Continued)

the bluff body - occur in the near-wake region of the bluff body. The ongoing APL experimental program involves both nonreacting and reacting situations, with air in the annular jet and with CO_2 or air or propane (for combusting flows) in the central jet.

The isothermal modeling predictions reported herein consider the influence of the annular and central flow rates and of the central-jet fluid on the nature of the flowfield downstream of the bluff body. The numerical computations are performed with the Field Relaxation Elliptic Procedure (FREP) Code. A constant effective eddy viscosity is employed in the calculations.

The numerical results have demonstrated the complex nature of the flowfield interactions in the near-wake region under different flow rates in the annular and central jets. The character of the flowfield emerging from the numerical predictions when the near wake is dominated by the annular jet or the central jet is in conformity with the APL experimental observations and with the heuristic description suggested therefrom.

The predicted results show good agreement for the overall trends and fair to poor quantitative agreement with the recent velocity and concentration measurements. The agreement is much better for the centerline location of the rear stagnation point than of the forward stagnation point. The predictions do not show the observed linear dependence of the forward stagnation point on the central-jet exit velocity. In the reverse-flow region behind the bluff body, the present numerical results show good agreement with the recent APL measurements and with the annular-jet data in the literature.

Despite the crude turbulent-viscosity model and the unity effective Schmidt number assumption employed in the predictive calculations, present results have served to refine the understanding of the APL combustor flowfields and to suggest fruitful avenues for future experimental and predictive efforts.

PREFACE

Accession For

By

Distribution/

Availability Codes

Dist	Avail and/or Special
A	

DTIC
SELECTED
SEP 2 1981

D

iii

TABLE OF CONTENTS

TABLE OF CONTENTS (Continued)

LIST OF ILLUSTRATIONS

LIST OF ILLUSTRATIONS (Continued)

LIST OF TABLES

LIST OF SYMBOLS

a_ϕ	Coefficient for the convection term (see Equation 3)
b_ϕ, c_ϕ	Coefficient for the diffusion term (see Equation 3)
d_ϕ	Coefficient for the source term (see Equation 3)
d	Diameter of the centerbody
d_f	Diameter of the central tube
D	Inner diameter of the confining duct
H	Stagnation enthalpy of mixture
I	Index of computational nodes in the axial direction
J	Index of computational nodes in the radial direction
M_i	Local mass fraction of species
r	Radial coordinate
U	Time-averaged radial velocity component
W, $\overline{W}$	Time-averaged axial velocity component
z	Axial coordinate
z_s	Axial coordinate of the centerline stagnation point
μ_{eff}	Effective turbulent viscosity
ρ	Local density of mixture
ϕ	Representative dependent variable (see Equation 3)
ψ	Stream function (see Equation 1)
ω	Vorticity (see Equation 2)

Subscripts

A	Annular exit plane
C	Velocity profile centerline
F	Central-jet exit plane

SECTION I
INTRODUCTION

Numerical prediction of recirculating, turbulent flowfields has been the subject of several studies in the recent past. These studies have considered steady or unsteady, and nonreacting or reacting flowfields involving single-phase and two-phase situations. The numerical computations of steady, recirculating flowfields under both isothermal and combusting conditions have been motivated in part by the need to model the fluid dynamic and combustion processes in gas turbine combustors.[1-7] Combustor modeling is still in a state of development and some of the areas requiring further refinement have been identified.[8] Nevertheless, some success has been achieved recently in applying the results of numerical modeling to actual combustor development activity.[4] Furthermore, recent validation studies[9-12] have shown that currently available combustor models are reasonably adequate for providing qualitatively correct descriptions of the recirculating flowfields. This report presents some numerical predictions of the isothermal flowfields in a research combustor that has been designed to simulate some elements of the primary zone of a gas turbine combustor.

1.1 BACKGROUND

An experimental and modeling program is in progress at the Aero Propulsion Laboratory (APL) of the Air Force Wright Aeronautical Laboratories for evaluating combustion models and diagnostic techniques in realistic environments. The major component of this research program is the axially symmetrical bluff-body-in-duct combustor (hereafter referred to as the centerbody combustor) employed to furnish point measurements of velocity, temperature, and specie concentrations in the recirculating, turbulent, near-wake regions.

1.1.1 APL Centerbody Combustor

The predictive modeling results reported here pertain to the centerbody combustor configuration. The details concerning the philosophy and selection of the combustor design, brief descriptions of the combustor facility and instrumentation, and the preliminary experimental results of the combustor development tests are available in Reference 13. In the absence of numerical predictions of the flowfields, the

interpretation of these experimental data utilized flowfield descriptions derived heuristically. Detailed discussions on these postulated flowfields are given elsewhere.[11] Despite the qualitative nature of the flowfield descriptions, it was noted that they provide a reasonably consistent framework for designing experiments for future model development and validation studies.[13]

Reference 11 has discussed at length the implications of the suggested flowfields on predictive modeling. It was stated there that detailed mapping of the velocity and concentration fields by diagnostic measurements and by numerical predictions would be essential before the flowfield in the centerbody configuration could be quantitatively established. The recent results of laser Doppler anemometry measurements[14] under both isothermal and combusting conditions have furnished information concerning the centerline axial velocity distributions in the near-wake region. These results have essentially confirmed the earlier flowfield descriptions. Thus, it is of interest to carry out the predictive calculations for the appropriate experimental conditions. As has been discussed previously,[11] even isothermal flowfield modeling should be of value in evaluating combustor models. Indeed, it was emphasized that only when the numerical model is able to predict the salient features of the isothermal flowfield can its capability to handle the additional complexities arising in reacting flows be established with confidence. Accordingly, the work reported here deals with the numerical predictions of the isothermal flowfields in the centerbody combustor under the conditions adopted for the previous experimental studies.[13,14]

The centerbody combustor consists of a 14-cm diameter cylindrical bluff body placed concentrically in a 25.4-cm diameter duct. The centerbody has a flat end face downstream and an aerodynamically shaped end face upstream. The centerbody has a length-to-diameter ratio of 5.6 so that nearly uniform velocity profiles are established at the inlet plane for the air flowing in the annular passage between the confining outer duct and the centerbody. Gaseous fuel (propane) or an inert gas (CO_2) is injected at the center of the centerbody downstream face through a 4.8-mm diameter tube. The central tube configuration adopted in the experiments[14] had insufficient length-to-diameter ratio for assuring a fully developed turbulent velocity profile at the tube exit. Future experiments would employ a convergent nozzle configuration to provide uniform velocity profiles at the exit.

2

In view of the particular geometry adopted, the centerbody combustor is essentially a dual coaxial flow configuration. However, the interjet separation is much larger than that usually encountered in typical dual jet flows.

1.1.2 Related Studies

The juxtaposition of the annular and central jets with the near-wake region behind the centerbody has given rise to some interesting ramifications not previously considered in numerical modeling. Indeed, for the centerbody configuration, experimental or predictive information is scanty in the published literature. The early work of Chigier and Beer[15] reported the measurements in the near-field region of double concentric jets. This configuration consisted of a central nozzle 2.5 cm in diameter and an annular nozzle having inner and outer diameters of 6.4 and 9.7 cm. The air flow from the annular and the central nozzles issued into ambient air and the flow downstream of the nozzles was unbounded. Although this work provided some insights that helped postulate the flowfields in Reference 13, significant differences exist between this configuration and the centerbody configuration. The annular air flow is confined and the diameter of the centerbody is an order of magnitude larger than the diameter of the fuel tube in the centerbody configuration. A careful examination of the more recent works on confined turbulent diffusion flames[16-19] reveals that these do not possess the significant features of the centerbody configuration. Only Elliman, et al.,[20] appear to have studied a configuration similar to the centerbody combustor. The combustor used in that study consists of an outer duct 150 mm in internal diameter and a disc baffle 125 mm in diameter. Air flows through the annular passage and methane through a central fuel tube. (Although the paper does not explicitly state the diameter of the fuel tube, it seems to be about 12.5 mm.) However, the flow pattern in this configuration is significantly affected by the 45° lip provided for the baffle and by the radially exhausting flow arrangement, situated at only 400 mm from the face of the baffle. Moreover, both the numerical predictions and the intrusive diagnostic measurements have dealt only with combusting flows. Finally, the recent papers by Ko and Chan[21-23] which deal with isothermal-flow measurements in annular jet flows (differing from the centerbody configuration by the absence of the central jet and the outer confining duct) provide some information on the location of the centerline reattachment point and vortex center. These aspects are dealt with in Section IV.

1.2 SCOPE OF PRESENT WORK

The present Senior Investigator program is a continuation of the earlier efforts[9-11] concerned with an examination of the two Air Force furnished computer

programs to evaluate their ability to predict the flowfields in the APL centerbody combustor configuration. The previous studies had demonstrated that the Field Relaxation Elliptic Procedure (FREP) Code had the capability of making reasonable quantitative predictions of the turbulent flowfield in an isothermal flow with imbedded recirculating regions. Accordingly, the numerical computations reported herein have been performed with the FREP Code. These predictive calculations have employed an appropriate value for the eddy viscosity coefficient which is determined essentially by trial and error. The numerical modeling has considered the experimental conditions adopted for the recent laser Doppler anemometry measurements. These conditions include several annular- and central-jet flow rates as well as different central-jet fluids. Present isothermal-flowfield predictions have generally supported the earlier postulated flowfields and have served to refine the fundamental understanding of the interactions between the annular and the central jets.

1.3 OUTLINE OF REPORT

A brief description of the FREP Code is given in Section II, which also outlines the computational procedure and the input requirements with respect to the centerbody configuration. Section III provides the details of the numerical computations. The results of the predictive modeling are discussed in Section IV. Finally, Section V outlines the conclusions of the present study and also offers recommendations for future activity.

SECTION II

MODELING DETAILS

The predictive modeling of the isothermal flowfields in the centerbody configuration is accomplished by numerically solving the time-averaged Navier-Stokes equations. The FREP Code employs a finite-difference computational procedure to solve the system of partial differential equations describing the conservation laws of mass, momentum, energy, and chemical species. Following is a brief discussion of the theoretical and computational aspects of the FREP Code.

2.1 GOVERNING EQUATIONS

The modeling in the FREP Code involves two-dimensional, steady-state flowfields in planar or axisymmetric geometries. Because of the geometry of the centerbody configuration, the present computations are concerned only with axisymmetric flowfield. Details concerning the FREP Code may be found in References 1 and 9.

In the numerical solution of the Navier-Stokes equations in the FREP Code, the vorticity and the stream function are employed as dependent variables. Thus, a direct solution of the primitive variables involving the velocities and pressure becomes unnecessary. For the axisymmetric geometry, the stream function ψ and the vorticity ω are defined as follows:

$$\psi = \int (\rho W r \, dr - \rho U r \, dz) \tag{1}$$

$$\omega = \frac{\partial U}{\partial z} - \frac{\partial W}{\partial r} \tag{2}$$

where U and W are respectively the radial (r-direction) and the axial (z-direction) time-mean velocity components. The other dependent variables are the stagnation enthalpy H, and the species mass fraction m_i. Two chemical species, air and fuel, are considered. The governing equation for all the dependent variables can be cast in the general form

$$a_\phi \left[\frac{\partial}{\partial z} \left(\phi \, \frac{\partial \psi}{\partial r} \right) - \frac{\partial}{\partial r} \left(\phi \, \frac{\partial \psi}{\partial z} \right) \right] - \frac{\partial}{\partial z} \left[b_\phi r \frac{\partial}{\partial z} \left(c_\phi \phi \right) \right]$$

$$- \frac{\partial}{\partial r} \left[b_\phi r \frac{\partial}{\partial r} \left(c_\phi \phi \right) \right] + r d_\phi = 0 \tag{3}$$

5

where the coefficients, a_ϕ, b_ϕ and c_ϕ, and d_ϕ represent respectively the convection, diffusion and source terms. All these coefficients for the general case are given in Table 1 of Reference 1. Certain simplifications are possible when the effective turbulent Prandtl and Schmidt numbers are assumed to be unity. Under this assumption the complicated source term d_ϕ for the stagnation enthalpy equation vanishes identically. For the species equation, the chemical reaction source term is excluded for the nonreacting flowfield under consideration. The coefficients appropriate for the present isothermal modeling are given below in Table 1. It may be noted that with unity turbulent Prandtl and Schmidt numbers, the turbulent exchange coefficients for the energy and species transport (b_ϕ terms) are replaced by the turbulent momentum exchange coefficient (or the effective viscosity) μ_{eff}. It is necessary to introduce a turbulence model for prescribing μ_{eff} in order to solve Equation (3). However, as concluded in Reference 11, the FREP Code is operational only with a simple constant eddy viscosity model. In the present numerical computations, the value of the constant eddy viscosity was arrived at by a trial and error approach; this aspect is discussed in Section III.

TABLE 1
COEFFICIENTS FOR THE DEPENDENT VARIABLES

ϕ	a_ϕ	b_ϕ	c_ϕ	d_ϕ
ψ	0	$1/(\rho r^2)$	1	$-\omega/r$
ω/r	r^2	r^2	μ_{eff}	$-r\left[\dfrac{\partial}{\partial z}\left(\dfrac{U^2 + W^2}{2}\right)\dfrac{\partial \rho}{\partial r} - \dfrac{\partial}{\partial r}\left(\dfrac{U^2 + W^2}{2}\right)\dfrac{\partial \rho}{\partial z}\right]$
H	1	μ_{eff}	1	0
m_i	1	μ_{eff}	1	0

2.2 COMPUTATIONAL PROCEDURE

Equation (3) represents a system of coupled, nonlinear partial differential equations. In view of the elliptic nature of the steady-state equations in two space dimensions, a

6

relaxation technique is employed in the numerical solution procedure. The FREP Code uses the residuals of the variables rather than the variables themselves in an iterative relaxation technique. The residuals are the deviations of the current solution at any stage in the iteration from the true solution of the finite-difference equations. A successive reduction of these residuals is carried out at each nodal point of a two-dimensional grid until a specified accuracy criterion is reached. The so-called Field Relaxation technique of the FREP Code is based upon the Peaceman-Rachford[24] form of the Alternating Direction Implicit method. The present modeling utilizes the predictor-step calculations of the Code and the rationale of this approach is discussed in References 9 and 11.

2.3 BOUNDARY CONDITIONS

The solution of Equation (3) requires the specification of appropriate boundary conditions for each of the dependent variables on all the boundaries of the computational domain. The computational domain under consideration for the centerbody configuration is shown schematically in Figure 1. Because of axial symmetry, only the top half of the combustor is employed in the computation. The top boundary represents the inflow boundary and consists of the fuel inlet port, the centerbody face, and the annular air inlet. The right boundary is the outflow boundary. The boundary conditions at the exit boundary presume the flow to be unidirectional there. However, the location of this boundary is unknown a priori and hence its specification is essentially arbitrary. In a given problem the location of the exit boundary is subject to the constraints of available computer memory and required spatial resolution.

The boundary conditions for the stream function, vorticity, stagnation enthalpy and species mass fraction are specified in terms of the coordinates tangential and normal to the boundary. The boundary conditions along the duct wall (top boundary) represent the no-slip conditions for velocity, zero normal mass flux for species, and prescribed wall temperature (cooled walls). The boundary conditions along the axis of symmetry denote symmetry conditions. The stream function value on this boundary is set at zero. For all other dependent variables the radial gradients are set at zero. At the exit boundary, the nearly unidirectional flow conditions are represented by vanishing second derivatives in the axial direction. Finally, it is necessary to prescribe the distributions of the axial and radial velocities and their gradients, as well as of the pressure, temperature, and fuel mass fractions at the inlet ports. In addition, at the top node of each of the inlet ports on the left boundary, the stream function value consistent with the inlet mass flux must be specified.
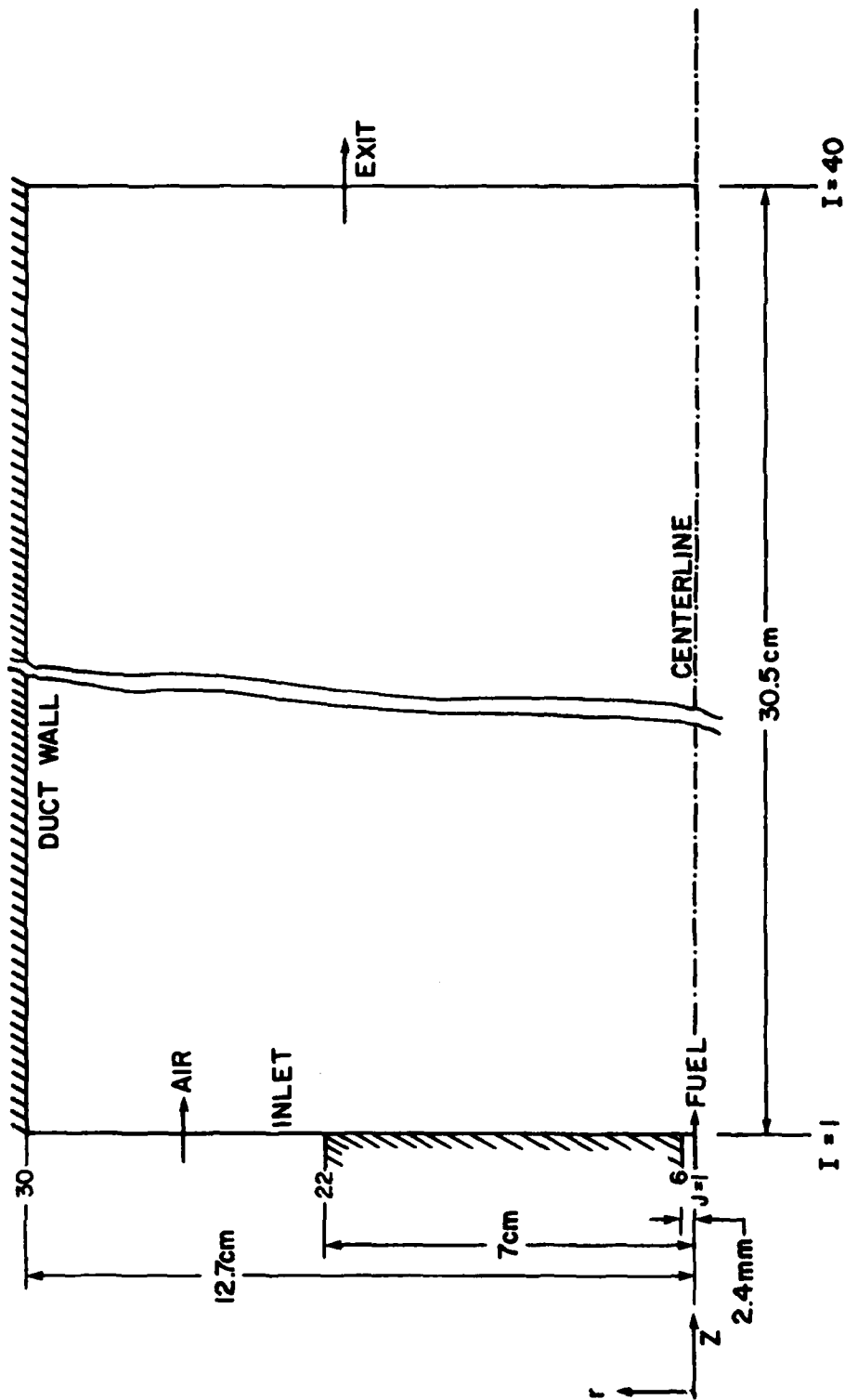
7

Figure 1. Computational Domain for the Centerbody-Combustor Flowfield Modeling.
(I: Axial Node Index J: Radial Node Index.)

2.4 INLET-VELOCITY DISTRIBUTIONS

As noted in paragraph 1.1.1, the design of the centerbody should assure a nearly axial flow at the inlet plane of the annulus. However, this conclusion has not been demonstrated by actual laser anemometry measurements of the radial velocity distribution in the inlet plane. The presence of finite radial velocity components has been observed in earlier investigations[20, 25] and it is likely that the centerbody configuration may exhibit similar characteristics. It should be noted that the prediction of downstream flow properties has been shown by Pope and Whitelaw[26] to be quite sensitive to the assumed initial profile of radial velocity. Thus, it is essential for numerical modeling to have accurate information on the radial velocity distribution at the inlet. In the absence of this information, the present calculations assume negligible radial velocity components in the inlet flow. The assumed axial velocity profiles at the inlet of the annular and central ports are shown in Figure 2. Each velocity profile is shown normalized with respect to its centerline velocity(W_c). The experimental conditions of the respective mass-flow rates serve to determine the absolute values of axial velocities, and these are employed to obtain the boundary value of the stream function discussed in paragraph 2.3. The assumption of a universal inlet velocity profile for all inlet mass-flow rates is clearly inadequate. Instead, the actual profile for any particular flow condition available from measurements must be used. Although the laser anemometry measurements are expected to furnish the annular inlet-plane velocities without much difficulty, at the fuel inlet, measurements no closer than 5 mm from the inlet plane appear likely. This experimental constraint makes it all the more desirable to have a fuel inlet configuration in the shape of a convergent nozzle which would provide a nearly uniform velocity profile at its exit.

2.5 COMPUTATIONAL GRID

For the two-dimensional computation domain seen schematically in Figure 1 the *distribution of grid nodes requires* considerable judgment, since this aspect is governed by two opposing constraints - required spatial resolution and available computer memory. In the FREP Code the user can specify either uniform or nonuniform axial and radial grid spacing. The region requiring the greatest attention in the centerbody configuration is the near-wake recirculation region behind the centerbody. A uniform grid spacing in the radial and axial directions with the available number of grid points would clearly result in too poor a spatial resolution. Thus, a nonuniform distribution of grid spacing is obviously indicated.

Preliminary calculations[9] on the centerbody configuration had established that the two-dimensional grid array of 28 axial nodes x 21 radial nodes available with the FREP Code

9
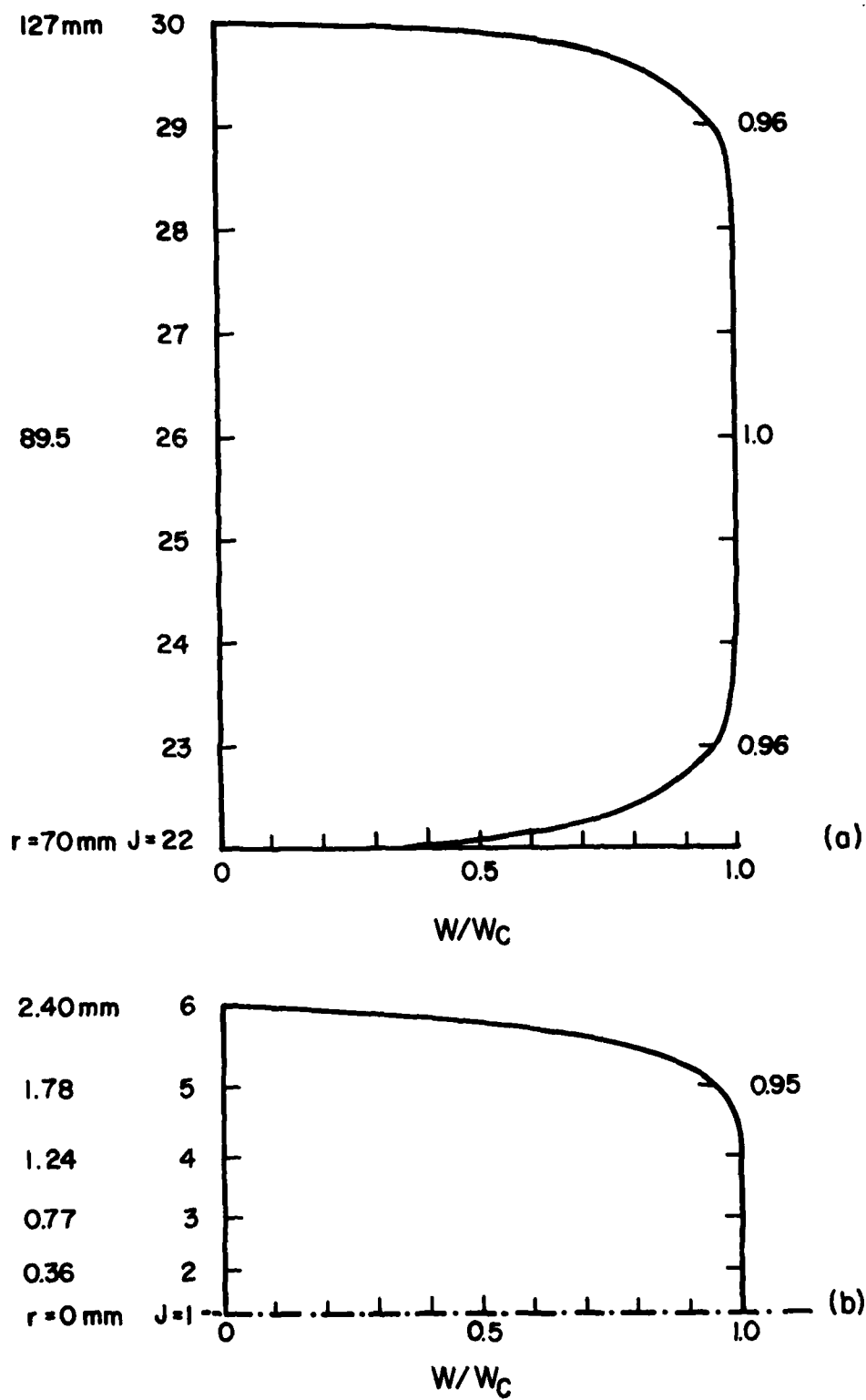
Figure 2.   Assumed Mean Axial Velocity Profiles at the Inlet Ports.
(a) Annular Port   (b) Central Port.

resulted in inadequate spatial resolution when an axial extent of 30 cm was used for the computational domain. Further trials indicated that a grid array of 40 axial nodes x 30 radial nodes would be the optimum for the FREP Code with an OVERLAY under the dual CDC CYBER systems available at the Aeronautical Systems Division computer center. This array requires a core memory of about $260,000_8$ words.

The distribution of grid nodes adopted in the present numerical predictions is as follows: In the radial direction, nodes 1 through 6 represented the fuel inlet port, nodes 6 through 22 represented the centerbody face, and nodes 22 through 30 represented the annular port. This resulted in five interior nodes in the fuel inlet and seven interior nodes in the air inlet. A nonuniform radial grid spacing is employed from nodes 1 through 22, ranging from a minimum of 0.36 mm to a maximum of 7 mm. For the eight radial spacings in the annulus, a uniform value of 7.125 mm is used. In the axial direction, the axial extent of 30.5 cm is covered by 40 nodes, distributed nonuniformly throughout. This resulted in the first axial spacing of 0.35 mm and the last axial spacing of 14.5 mm. The initial axial spacings and the initial radial spacings (up to the 17th node in either direction) are of the same order. For example, 9 grid nodes cover a radial distance of 5.4 mm and an axial distance of 5.95 mm. This is a necessary requirement in view of the elliptic nature of the governing equations. It is seen that towards the top and right boundaries of the computational domain, the grid spacings are rather large. Unfortunately, this is unavoidable in the context of the limited number of grid points available. However, the present grid distribution represents the optimum choice and the grid spacing toward the exit boundary is not too crude to affect the flowfield everywhere.

SECTION III

NUMERICAL COMPUTATIONS

The predictive modeling of the isothermal, recirculating flowfields in the centerbody configuration has been conducted with the FREP Code employing a constant eddy viscosity model. A variety of experimental conditions involving different annular and central flow rates was simulated in the numerical calculations.

3.1 PRELIMINARY CALCULATIONS

The selection of stream-function boundary value and the choice of eddy viscosity necessitated trial calculations initially. These are briefly discussed in the next two paragraphs.

3.1.1 Stream-Function Boundary Values

It was noted in paragraph 2.3 that the boundary values of stream function consistent with the inlet mass fluxes of the annular and central jets must be prescribed. For the strictly axial inlet velocity profiles under consideration here, it is easy to see from the definition of stream function in Equation (1) that the difference in stream function values between two radial positions r_1 and r_2 is given by

$$\Delta \psi_{r_1 - r_2} = 2\pi \int_{r_1}^{r_2} \rho W r \, dr \quad . \tag{4}$$

Thus, denoting the stream function value to be zero at the centerline ($r=0$), the boundary value at the radial node $J=6$ can be computed from the central jet mass-flow rate. Since there is no mass flux through the centerbody face between the nodes $J=6$ through 22, the boundary value does not change. The boundary value at the $J=30$ node is computed from the air mass-flow rate. However, earlier experience with the FREP Code [9-11] had shown that a trial and error procedure is required for prescribing the stream-function boundary value. This is nescessary for obtaining a computed velocity distribution for the initial estimate (0th iteration) which would agree closely with the input velocity distribution (such as that shown in Figure 2). Too high a stream-function boundary value caused much larger inlet

12

velocities and too low a value resulted in much smaller (and sometimes even negative) velocities. Once the upper- and lower-bound values were established, the input velocity profiles could be zeroed in, within a few trials. Also, the dependence is essentially linear and thus the correct stream-function boundary values are obtained for other flow rates without a number of trials. The final stream-function boundary values corresponding to the different flow rates and the appropriate inlet-profile centerline velocities are shown in Table 2.

TABLE 2
BOUNDARY VALUES OF INLET VELOCITIES AND STREAM FUNCTIONS

Boundary Values	Fuel Flow Rate kg/hr / Air Flow Rate kg/s	2	0.07	0
ψ_6		0		
ψ_{30}	0	6.8082×10^{-1}		
W_1, m/s		0		
W_{26}, m/s		48.13		
ψ_6		3.3465×10^{-4}	3.3465×10^{-4}	3.3465×10^{-4}
ψ_{30}	4	6.8115×10^{-1}	2.4163×10^{-2}	3.3465×10^{-4}
W_1		34.37	34.37	34.37
W_{26}		48.13	1.685	0
ψ_6		5.0188×10^{-4}	5.0188×10^{-4}	5.0188×10^{-4}
ψ_{30}	6	6.8132×10^{-1}	2.4330×10^{-2}	5.0188×10^{-4}
W_1		51.54	51.54	51.54
W_{26}		48.13	1.685	0
ψ_6		6.6910×10^{-4}	6.6910×10^{-4}	6.6910×10^{-4}
ψ_{30}	8	6.8148×10^{-1}	2.4498×10^{-2}	6.6910×10^{-4}
W_1		68.71	68.71	68.71
W_{26}		48.13	1.685	0

3.1.2 Constant Turbulent Eddy Viscosity

The choice of the constant value for eddy viscosity in the centerbody flowfield is made only by trial and error. Prior modeling calculations on a dump combustor[10] and the algebraic modeling from Gosman, et al.,[27] provide a reasonable basis for the initial guess. The proper choice of the eddy viscosity is determined by a few trial computations and is governed by considerations such as the rate of convergence of the computed solutions, and the presence and extent of the recirculation region. It is known from experiments that the centerline reattachment point for the bluff-body vortex occurs at roughly one bluff-body diameter downstream. This observation has been utilized to facilitate the selection of optimum eddy viscosity. Further refinements take into account the behavior of the numerical solutions. The trial computations indicated that the rate of convergence becomes insensitive when the eddy viscosity value lies between 0.149 and 0.223 g/cm-s (1×10^{-2} and 1.5×10^{-2} lbm/ft-s). Most of the reported results here are based on eddy viscosity value of 0.149 g/cm-s.

It should be emphasized that turbulent eddy viscosity, being dependent on the flowfield, can not be a constant when significant variations in the velocity gradients occur throughout the flowfield. Also, the injection rates of the annular and central jets do influence the near-wake flowfield and this should be taken into account. However, there is no firm basis for incorporating these considerations into the obviously crude constant eddy-viscosity model. Indeed, the deficiency of this model became apparent when the numerical computations involving much higher central-jet flow rates (which would cause the central jet to penetrate the recirculation region) failed to converge and ran into severe numerical instabilities.

3.2 CASE STUDIES

The predictive calculations generally conformed to the experimental conditions of the recent laser anemometry measurements.[14] The cases for which the results are reported here are identified in Table 2. A convergence criterion of 5×10^{-3} for the relative residuals was employed in these calculations. Typically, this level of convergence was attained in 30 to 35 iterations. Each iteration took about 50 seconds of CP time on the CDC CYBER 175 computer.

3.2.1 Annular Air Mass Flow of 2 kg/s

Computations have been completed for the central jet CO_2 mass flows of 0, 4, 6, and 8 kg/hr. The last three cases pertain to the annular-jet dominant flow regimes of

14

Reference 13. Computations for central-jet flow rates of 10, 12, and 16 kg/hr failed to yield converged solutions. For the annular air mass flow of 2 kg/s, a set of three cases was computed for which the central-jet fluid was air instead of CO_2. This was done to verify the experimental observation[14] wherein the centerline location of the fuel stagnation point is dependent only on the central-jet exit velocity and not on the central-jet fluid. The calculations with air as the central-jet fluid were done for the same values of the central-jet exit velocity as for the CO_2 flow rates of 4, 6, and 8 kg/hr. This was easily accomplished by changing the stream-function boundary value to account for the different densities of CO_2 and air.

3.2.2   Annular Air Mass Flow of 0.07 kg/s

Since the computations outlined in paragraph 3.2.1 did not include the flow regime wherein the central jet was dominant, it was of interest to consider another set of flow conditions which would simulate this regime. In the laser anemometry measurements, annular air-flow rates of the order of 0.07 kg/s are the minimum needed to keep the seed particles from coating the window. Thus, flowfield computations with such a low air mass flow are in order. These calculations involved central-jet flow rates of 4, 6, and 8 kg/hr of CO_2. The same value of eddy viscosity which provided convergent solutions for the case in paragraph 3.2.1 was found acceptable for the cases here in which the central jet is dominant. Also, the computations with 16 kg/hr for the central jet failed to converge again. Thus, the numerical problems encountered with high central-jet flow rates do not seem to be related to the existence of different flow regimes.

3.2.3   Zero Annular Air Mass Flow

An examination of the decay of the centerline axial velocity for the cases studied in paragraph 3.2.2 showed that even under very low annular air flows, there was not the expected monotonic decay. The axial variation of the axial velocity on the centerline exhibited a minimum. Thus, it was clear that the presence of the centerbody was noticeable under nonzero annular flows. To examine the behavior of the central jet when the annular jet is completely absent, a set of three computations was performed with CO_2 central-jet flow rates of 4, 6, and 8 kg/hr.

SECTION IV

RESULTS AND DISCUSSION

The results of the predictive calculations outlined in the previous section are presented and discussed in the following paragraphs.

4.1 ANNULAR-JET DOMINANT FLOW REGIME

Following are the results of flowfield calculations when the central jet is completely dominated by the recirculating flow of the annular jet behind the centerbody. The annular air mass flow for all the cases considered here was 2 kg/s. In addition to the CO_2 flow rates of 4, 6, and 8 kg/hr in the central jet, the case where the central jet is absent also comes under this category. The computed flowfields with air in the central jet were similar to those with CO_2 in the central jet. Hence the former are not presented here. However, when the influence of central-jet fluid on the centerline stagnation points is discussed in paragraph 4.1.3.3, the relevant results of the calculations with central air jet are reported. The predicted results on stream function and axial velocity fields are discussed in the next three paragraphs and those on concentration fields are discussed in paragraph 4.3.

4.1.1 Stream-Function Fields

The predicted stream-function contours are shown in Figures 3 through 6. Figure 3 depicts the flow pattern when there is no central-jet flow. A toroidal recirculation region is set up behind the centerbody with a reverse flow along the centerline. The zero stream function contour separates from the centerbody surface and meets the centerline about 1.15 centerbody diameter downstream. This is the rear stagnation point. The forward stagnation point is, of course, at the center of the bluff-body face. Also shown is the computed zero axial velocity contour, which intersects the centerline at the rear stagnation point. Several closed contours confined between the centerbody face and the zero stream function contour represent the recirculating vortex.

It is of interest to compare the reattachment distance for the case of zero flow in the central jet with available experimental data. For the centerbody configuration, the recent measurement[14] shows that the reattachment point occurs at a z/d of approximately 0.9. Present calculations provide a value of 1.15. The results of Durao and Whitelaw[25] for the flow of an annular jet behind a disk show that for an annular diameter of 20 mm and different disk diameters of 8.9, 12.5, and 14.2 mm, z_s/d (z_s is the distance of reattachment point from the disk face) varies from 1.45 to 1 for initial velocities ranging
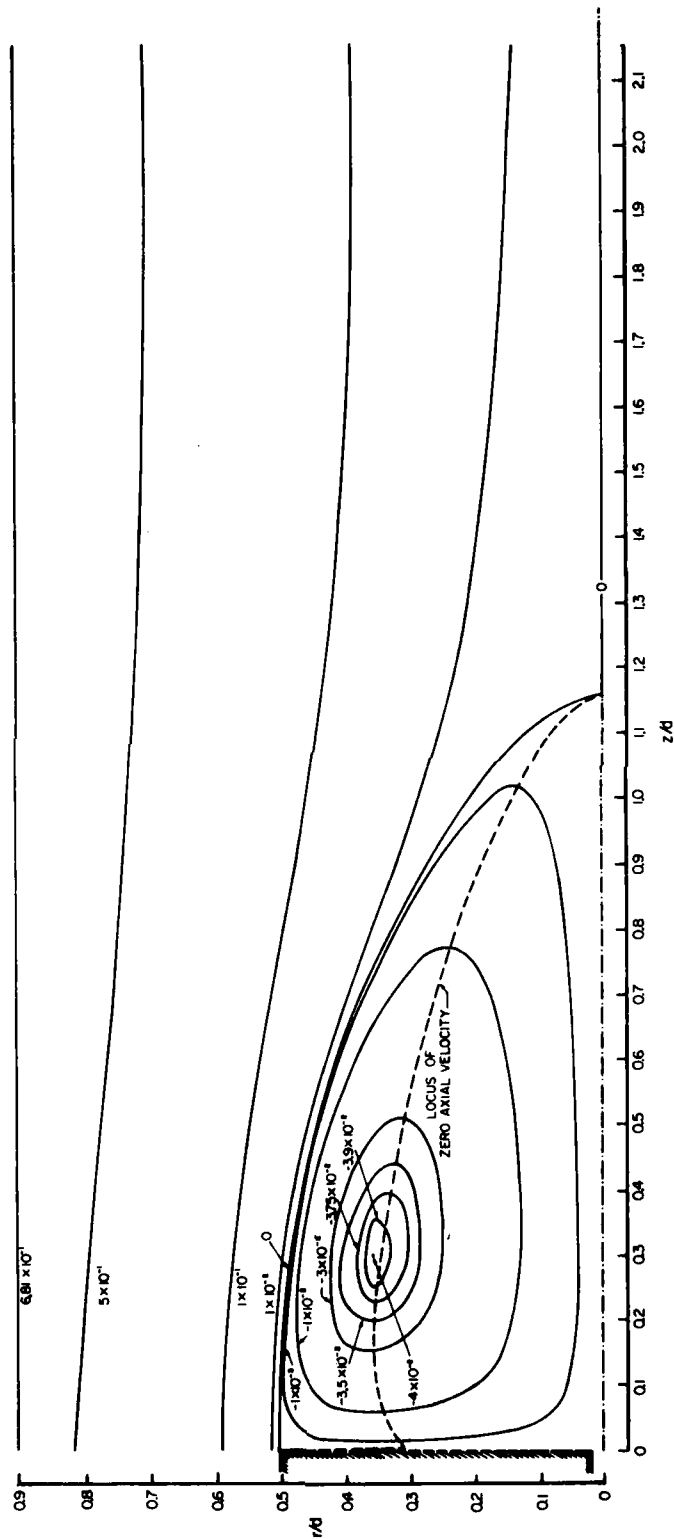
16

Figure 3.   Stream-Function Contours/2 kg/s Air Flow - Zero CO_2 Flow.
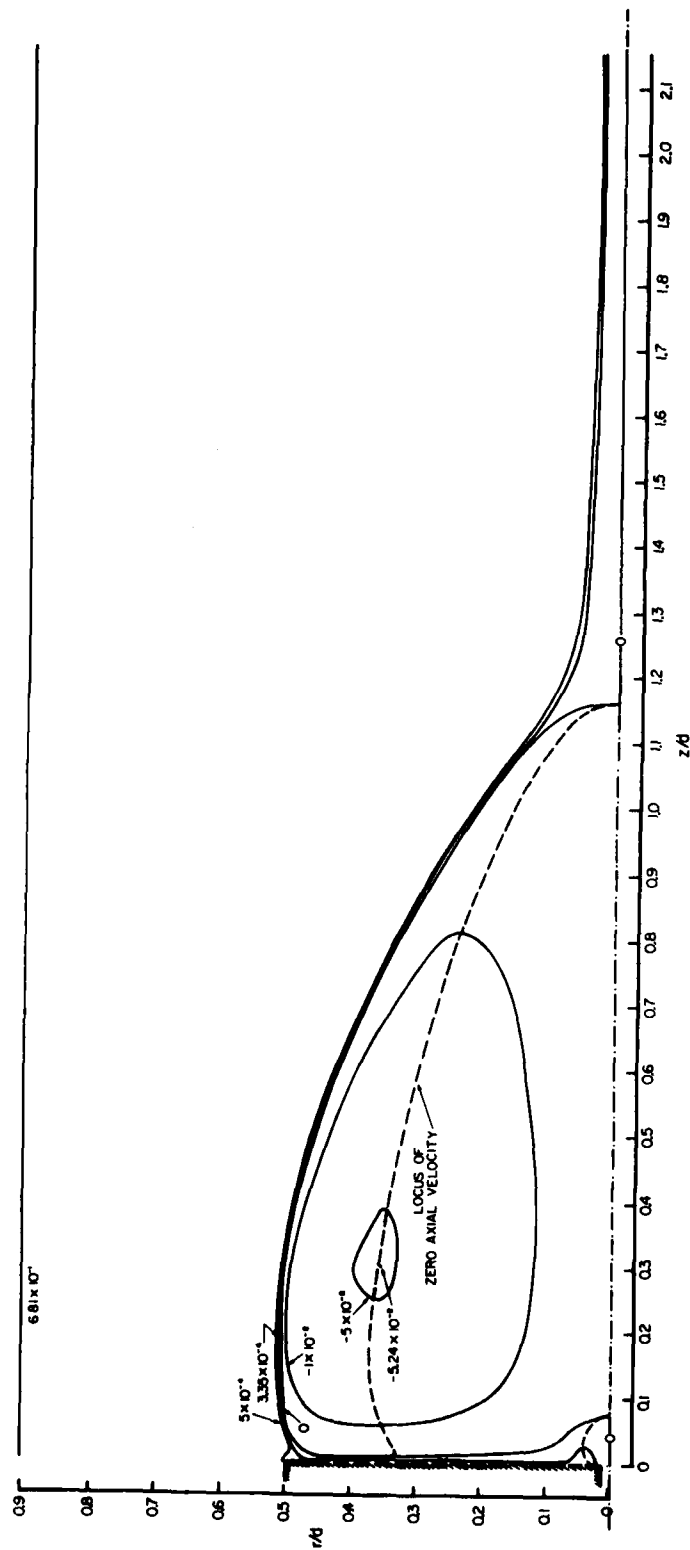
17

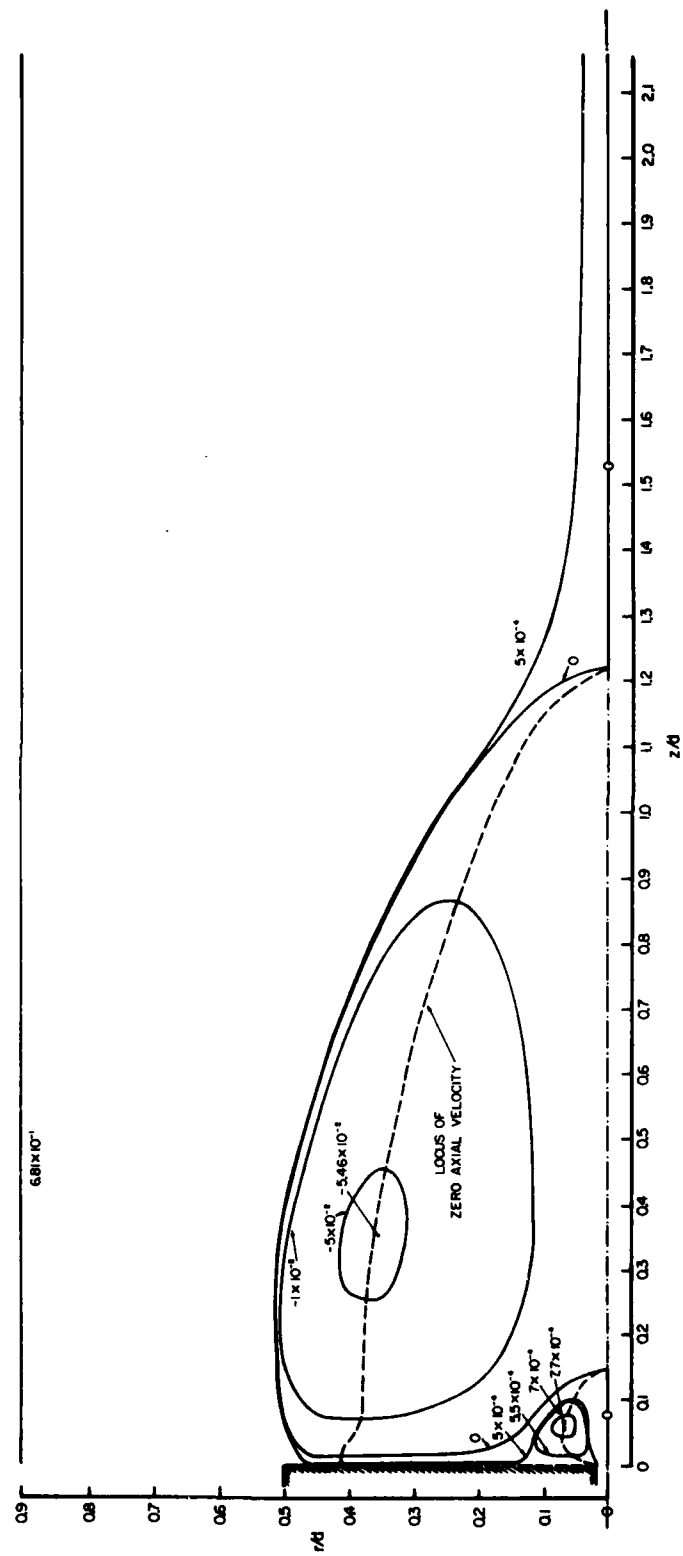Figure 4. Stream-Function Contours/2 kg/s Air Flow - 4 kg/hr CO_2 Flow.

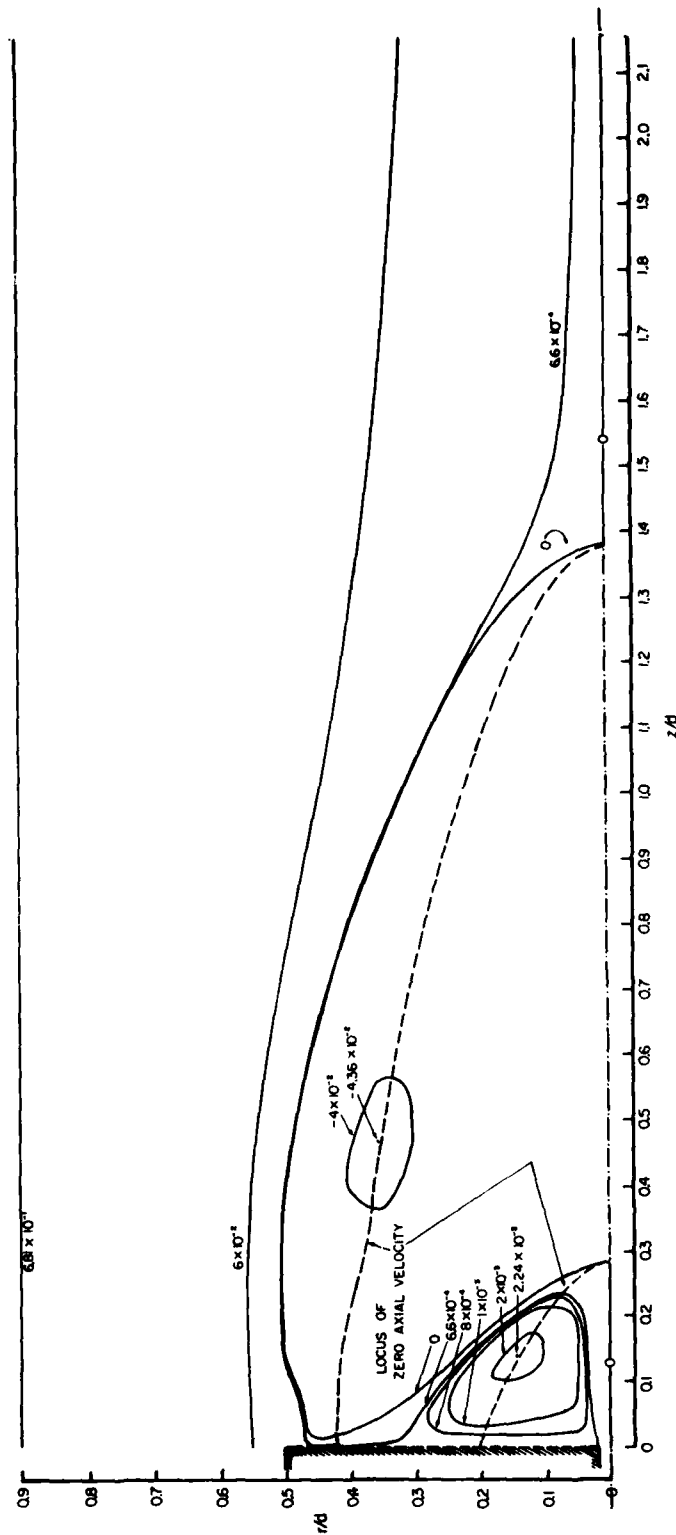Figure 5.   Stream-Function Contours/2 kg/s Air Flow - 6 kg/hr CO_2 Flow.

19

Figure 6. Stream-Function Contours/2 kg/s Air Flow – 8 kg/hr CO_2 Flow.

20

from 9.4 to 39.5 m/s. The greatest deviation from unity occurs for the largest values of the ratio of annulus diameter to disk diameter. For the centerbody configuration, this ratio (D/d) is 1.82, for which the data of Reference 25 suggests a value between 1.15 and 1.45 for z_s/d. The present numerical results and the earlier measurements[14] on the centerbody configuration indicate that this configuration is quite different even when no central jet is present. A similar conclusion is established from the results of Chigier and Beer,[15] and Ko and Chan[21] on annular jets (see Figure 3 of Reference 21, for example).

The character of the flow pattern changes when the central jet is introduced, as seen in Figures 4 through 6. The forward stagnation point on the centerline gets shifted downstream as the central-jet flow rate is increased. For the lowest central-jet flow rate of 4 kg/hr, although the rear stagnation point has moved slightly downstream, the near-wake flowfield (Figure 4) remains essentially the same as that of zero central-jet flow (Figure 3). However, at central-jet flow rates of 6 and 8 kg/hr, Figures 5 and 6 show the more dramatic changes in the near-wake flowfield. Another vortex of opposite sense begins to grow near the central-jet exit. Both forward and rear stagnation points are shifted further downstream.

Figures 3 through 6 also show the changes in the strength and growth of the two vortices. It is seen that the vortex center is identified by the extremum value of stream function. A local minimum (negative maximum) value is associated with the vortex caused by the annular flow and a local maximum value is associated with the vortex caused by the central-jet flow. From the definition of stream function in Equation (1), it can be seen that at the vortex center both the axial and radial velocity components vanish and hence the vortex center could be located by the intersection of zero axial and radial velocity contours. It should be noted that although the zero axial velocity contour in Figure 3 passes through the vortex center, the indicated negative maximum stream-function value is that available for a computational grid node. It is seen from Figures 4 through 6 that the strength of the negative vortex first increases, reaches a maximum, and then decreases as the central-jet flow rate is increased. The strength of the positive vortex, on the other hand, increases with increasing central-jet flow rate. This latter observation is consistent with the fact that as the central-jet flow rate increases, its entrainment requirement increases, which is met by the increased vortex strength. For the negative vortex, however, a more complex dependence is created by the presence of both annular and central jets, one of which tends to increase its strength whereas the other tends to diminish its importance.

An interesting observation can be made regarding the location of the center of the negative vortex. It is seen that as the central flow rate increases, the axial coordinate

21

of the vortex center moves downstream. But the radial coordinate appears to remain constant at a value of 0.35 for r/d. In terms of the duct diameter, the radial coordinate is 0.19. Ko and Chan[23] report a value of 0.18 for their annular jet configuration which has no central jet. Their study has shown that the radial position of the vortex center is essentially independent of the nondimensional parameter that represents the momentum flux of the annular jet and hence the pressure available for the entrainment behind the interface. Present numerical results with even a nonzero central jet confirm this observation and thus indicate that in the annular-jet dominant flow regime the central jet does not significantly affect the radial location of the vortex center.

The results of Ko and Chan[23] for the axial position of the vortex center show that the axial coordinate decreases with increasing nondimensional momentum flux of the annular jet. In other words, with higher momentum flux available from the annular jet, higher entrainment occurs in the region behind the centerbody face, resulting in the vortex moving closer to the face. It should be noted here that the present numerical calculations for constant annular flow rate do not provide for the variation in annular momentum flux. On the other hand, the variation of central-jet flow rate does affect the entrainment requirements behind the centerbody. It is physically logical that with greater momentum flux available from the central jet, less entrainment of the annular jet would occur. This necessarily implies that the vortex moves further downstream from the centerbody face. Thus, the present numerical results which show an increase in the axial coordinate of the vortex with an increase in the central-jet flow rate are physically consistent with the results of Ko and Chan.[23] Although the variation of the axial coordinate of the negative vortex in the present configuration shows qualitative agreement with the results of Reference 23, no simple correlation solely in terms of the annular-jet momentum flux is possible when a central jet is also present.

The computed results for the positive vortex caused by the central jet indicate that both the axial and radial coordinates of the vortex center increase with increasing central-jet flow rate. This observation raised the possibility that a suitable correlation could be found for the axial coordinates of both positive and negative vortex centers. It appeared that the negative vortex center moves downstream by the same amount as the positive vortex center when the central-jet flow rate is increased. In other words, the axial distance between the two vortex centers may be an invariant. A closer examination of the computed results, however, has shown that the axial distance between the centers increases nonlinearly with increasing central-jet flow rate. Additional parametric results are necessary for quantifying this dependence.

4.1.2 Axial Velocity Contours

Figures 7 through 10 present the predicted results of the mean axial velocity fields. The isovelocity contours represent velocities normalized with respect to the annular inlet velocity. Figure 7 shows the results when the central jet is absent. The intersection of the zero velocity contour with the centerline occurs at a z/d of 1.15. This is the rear stagnation point. The effect of increasing central-jet flow is seen in Figures 8 through 10. Due to the injection of the central jet fluid, a forward stagnation point is seen to occur on the centerline.

The numerical results clearly indicate that as the central-jet flow rate increases, both the forward and rear stagnation points on the centerline move downstream. This behavior is physically consistent. Recent experimental data[14] have shown that the forward stagnation point shifts downstream linearly with the central-jet exit velocity. Present numerical results underpredict the distances to forward stagnation points and also do not reveal any linear dependence on the exit velocity. Thus, for central-jet flow rates of 4 and 8 kg/hr of CO_2, the calculated z/d values for the centerline forward stagnation point are 0.08 and 0.28, while the measured values are 0.3 and 0.5. On the other hand, present computations overpredict the distances to rear stagnation points. The calculated z/d values for the rear stagnation point vary from 1.15 for zero central flow to 1.38 for 8 kg/hr central flow, while the measured value is 0.9 and within the precision of the measurements, the downstream movement of the rear stagnation point with increasing central-jet flow is not discernible.

Figures 7 through 10 furnish additional insights into the structure of the recirculation region. The contours of the negative axial velocity provide a measure of the extent and strength of the reverse-flow regions. Consider, for example, the contour representing the negative axial velocity of 50% of the annular inlet velocity. An inspection of Figures 7 through 10 reveals that as the central flow rate is increased from 0 to 8 kg/hr, both the axial and radial extent of this particular velocity contour increase, reach a maximum, and then begin to decrease. Indeed, the implication is clear that the strength of the reverse flow first increases, and then begins to decrease. Recalling the earlier observations on the strength of the negative vortex in Figures 3 through 6, it is easy to see that when the central-jet flow rate is increased, initially the dominance of the annular jet increases (Figures 7 and 8); then the dominance of the annular jet attains a maximum (Figures 8 and 9); and finally, the annular jet begins to get less dominant

Figure 7. Mean Axial Velocity Contours/2 kg/s Air Flow – Zero CO_2 Flow. (Velocities are shown normalized with reference to the annulus inlet-plane velocity.)

24

Figure 8.   Mean Axial Velocity Contours/2 kg/s Air Flow - 4 kg/hr CO_2 Flow.
(Velocities are shown normalized with reference to the annulus inlet-plane velocity.)

25

Figure 9.   Mean Axial Velocity Contours/2 kg/s Air Flow - 6 kg/hr CO_2 Flow. (Velocities are shown normalized with reference to the annulus inlet-plane velocity.)
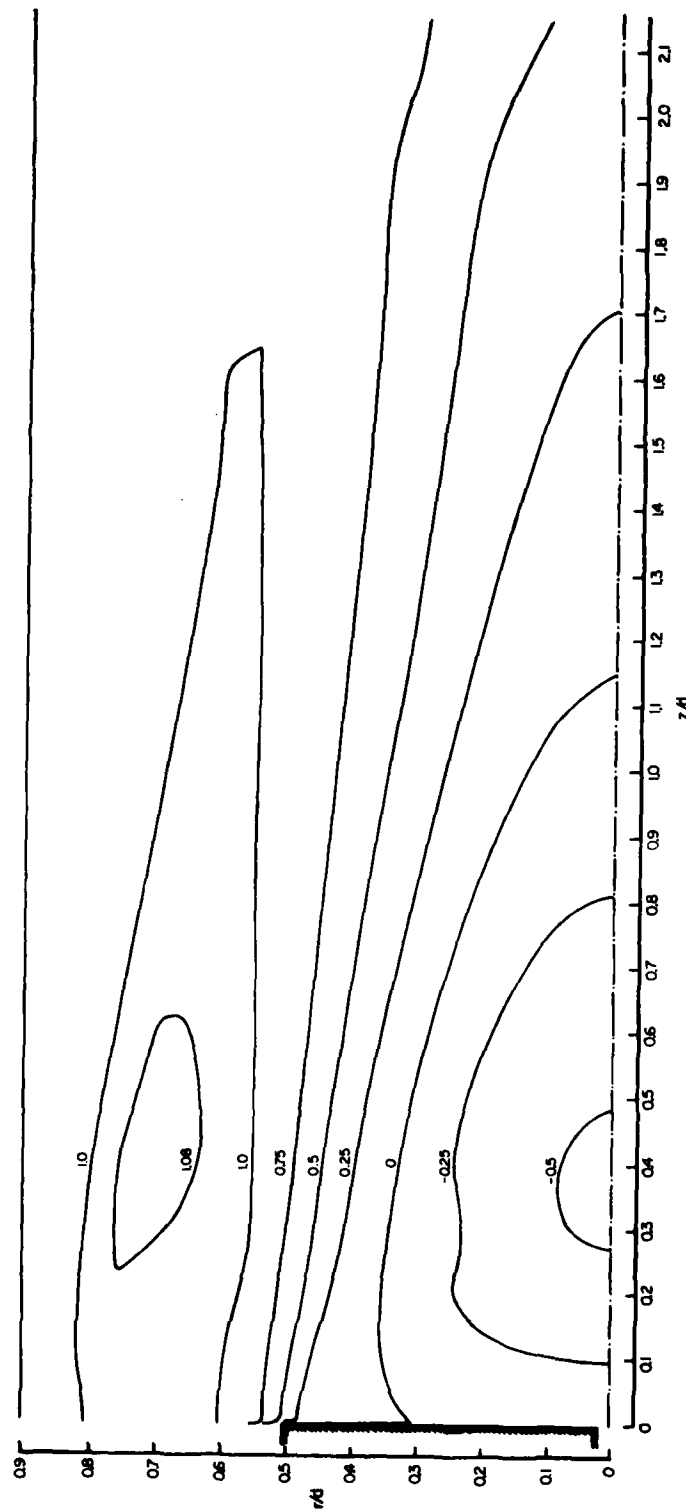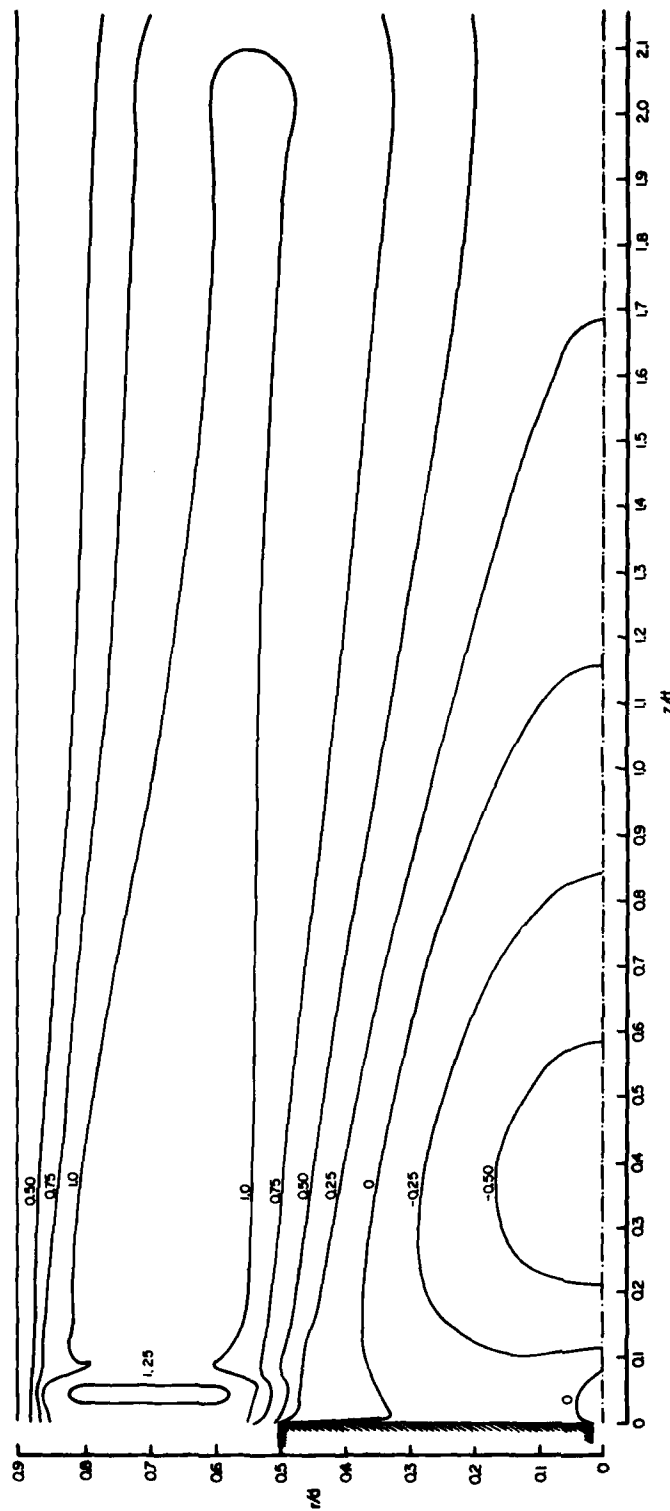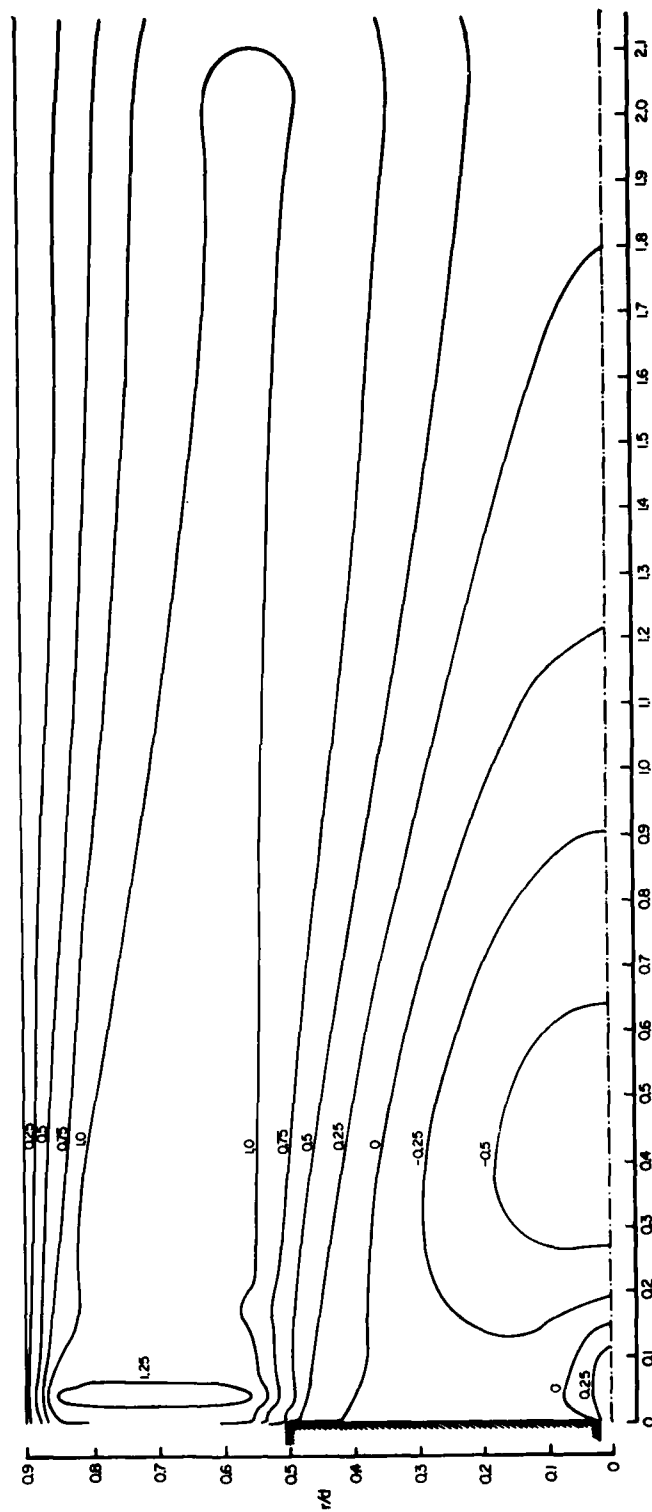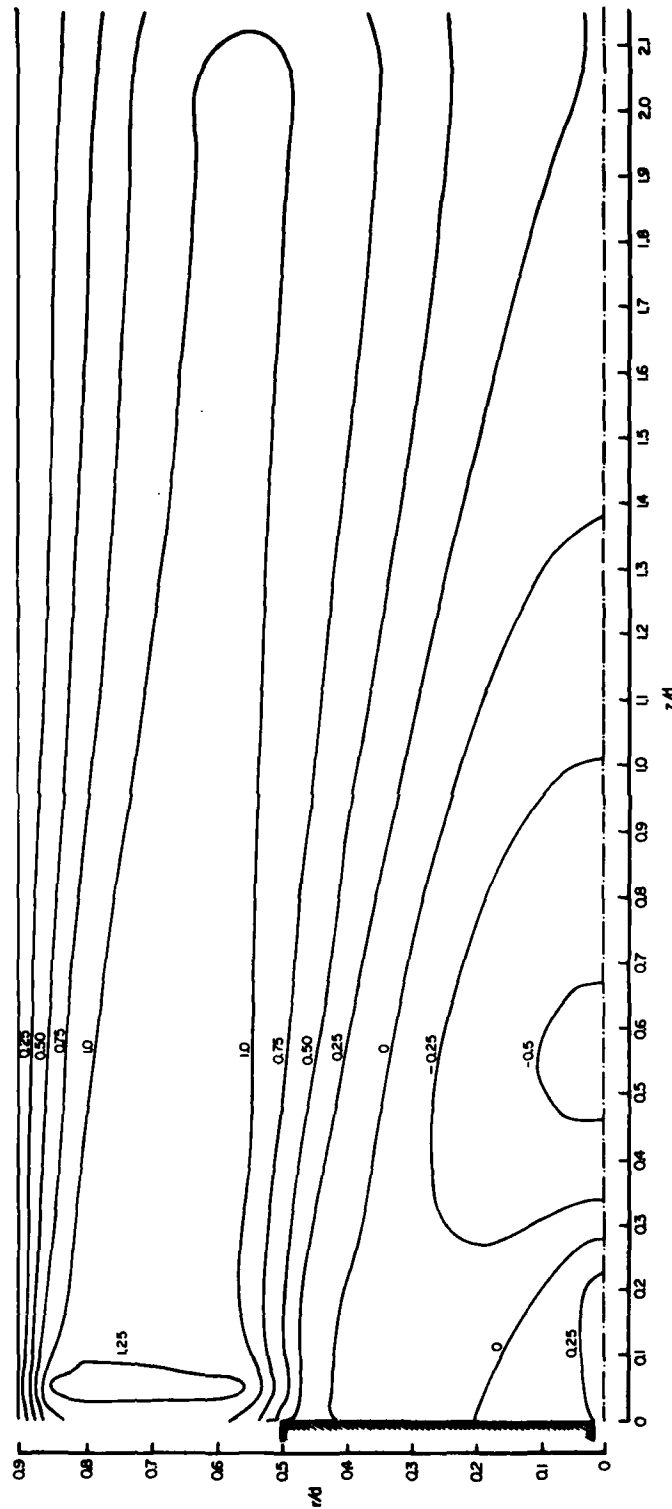
Figure 10. Mean Axial Velocity Contours/2 kg/s Air Flow – 8 kg/hr CO_2 Flow. (Velocities are shown normalized with reference to the annulus inlet–plane velocity.)

(Figures 9 and 10). This aspect of the recirculation-zone structure is further exemplified in the discussion of the centerline velocity characteristics in Paragraph 4.1.3.

The predicted isovelocity contours exhibit an interesting behavior of the annular jet. Figure 7 shows that downstream of the annular inlet plane, there is a slight acceleration of the annular jet in the core region. For the isothermal flow under consideration here, in view of the sudden expansion, this observation appears somewhat surprising. The acceleration is more pronounced in Figures 8 through 10 where immediately downstream of the inlet plane an increase of about 25% in axial velocity is seen. The reason for this observation is unclear at this time. In fact, it would be useful to see if measurements can show this phenomenon to be real.

4.1.3 Axial Variation of Mean Axial Velocity

Further elucidation of the structure of the recirculation region is possible by an examination of the axial velocity characteristics along the axial direction in the near-wake region. The variation of the axial velocity along the centerline is shown in Figure 11.

4.1.3.1 Centerline Velocity Profiles

A comparison of the predicted centerline results with the measured data (see Figure 4 in Reference 14) indicates good agreement in the overall trends. But in several specific results there is considerable disagreement. For central-jet flow rates of 4 and 8 kg/hr of CO_2, the forward stagnation point on the centerline was found to occur at a z/d of 0.3 and 0.5 in the experiments, compared to 0.08 and 0.28 in the predictions. Moreover, the computed results also do not show the linear dependence of the forward stagnation point on the central-jet exit velocity that was observed in the experiments.

The maximum negative velocity in the reverse-flow region was measured to be about 42% of the annular inlet-plane velocity and was found to occur at a z/d of 0.4. The predicted maximum, on the other hand, is 62% and occurs at a z/d of 0.38. Here the agreement is much better than that for the forward stagnation point. However, a physically more satisfying picture of the reverse-flow region emerges from the predictions in Figure 11. The velocity profiles for the four central-flow rates considered remain distinct, while in the measurements[14] all the velocity profiles coalesce beyond the maximum negative velocity. In other words, the measured velocity profile for zero central flow appears to envelope the velocity profiles for all central-flow rates from 4 to 12 kg/hr between the peak negative velocity location and rear stagnation point. Thus, the rear stagnation point is found to occur at a z/d of 0.9 and is independent of the central-flow rate. This
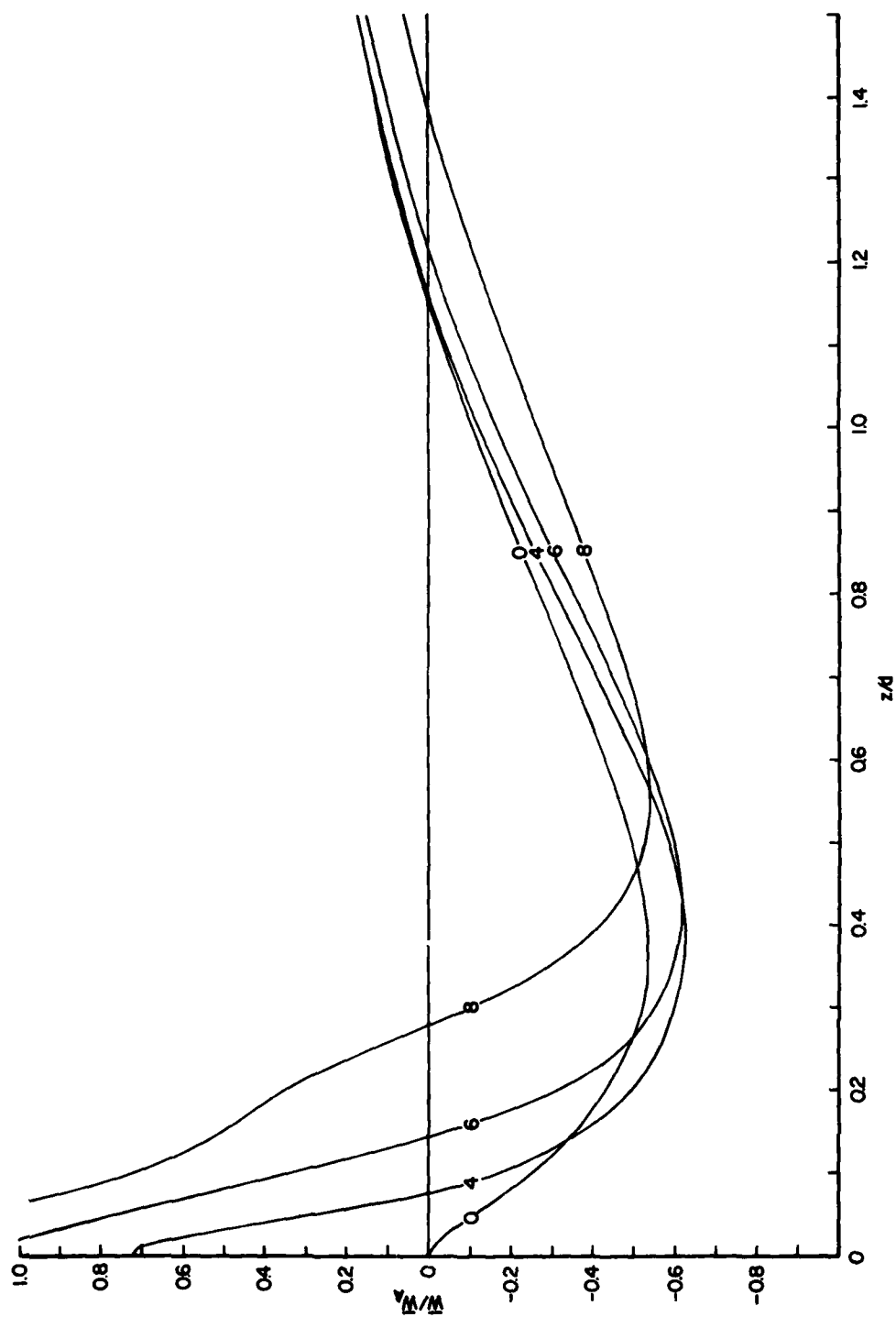
Figure 11. Axial Variation of Centerline Axial Velocity/2 kg/s Air Flow.
(The numbers denote central-jet flow rates of CO_2 in kg/hr.)

observation is somewhat inconsistent with the physics and is certainly less appealing intuitively. Possibly, the precision of measurements in the rear stagnation region is less than adequate.

The predicted location of the rear stagnation point varies from a z/d of 1.15 for zero central flow to 1.38 for 8 kg/hr central flow. The rear stagnation point for 4 kg/hr has only moved very slightly downstream from that for zero central flow. This shows that the recirculation region remains essentially unaffected by small central flow. It can also be seen from Figure 11 that the axial extent of the recirculation region (the distance between the forward and rear stagnation points) tends to decrease with increased central-flow rate.

The amplitude and location of the peak negative velocity provide additional insights into the structure of the recirculation region. The location of the negative peak moves from a z/d of 0.35 for zero central flow to 0.55 for 8 kg/hr central flow. This observation is consistent with physics in that the increasing central flow rate results in further penetration of the central jet inside the near-wake region and thus tends to decrease the influence of the reverse air flow for a greater distance downstream from the centerbody face. The variation of the amplitude of the peak negative velocity is more interesting. For zero central flow, this peak is about 53% of the annular inlet-plane velocity. The peak reaches a maximum of about 62% for 4 kg/hr central-flow rate, decreases slightly at 6 kg/hr, and then drops to about 53% at 8 kg/hr flow rate. Thus, the centerline variation of axial velocity discussed here confirms the previous notions outlined in Paragraphs 4.1.1 and 4.1.2 regarding the changing influence of the central jet as its flow rate is increased.

4.1.3.2 Off-Centerline Velocity Profiles

Figure 12 shows the predicted velocity profile in the axial direction 1 cm radially outward from the centerline. A comparison of Figures 11 and 12 reveals that the off-centerline profiles differ little from the centerline profiles everywhere except for the initial region corresponding to a z/d of about 0.2 from the centerbody face. Indeed, the locations and magnitudes of the peak negative velocity appear to be essentially identical. The locations of rear stagnation points also do not differ significantly. Of course, the off-centerline locations are closer to the centerbody face than the centerline locations, as can be seen from the isovelocity contours in Figures 7 through 10 and can be anticipated on physical grounds. It is clear from the isovelocity contours for central flow rates other than
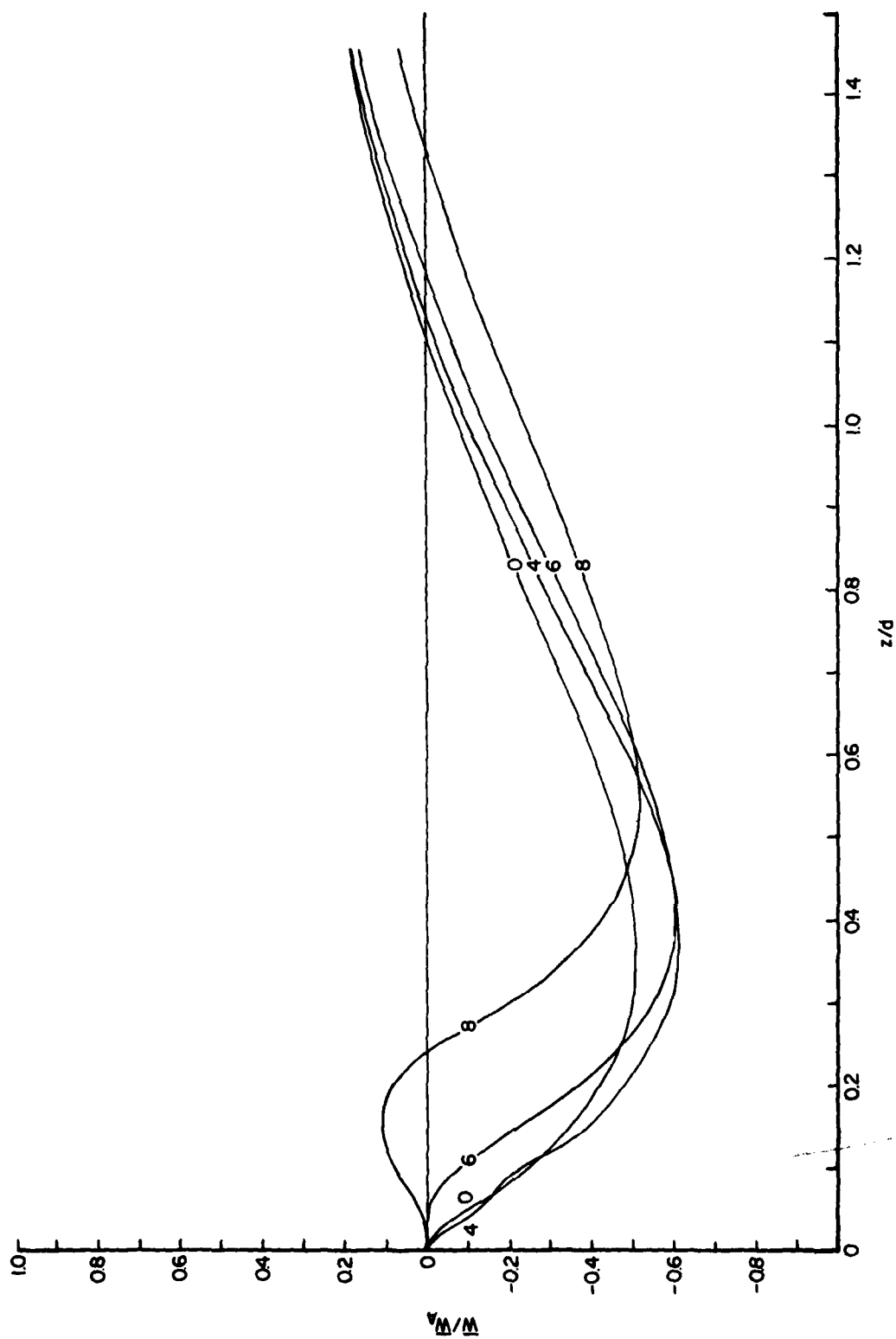
Figure 12. Axial Variation of Off-Centerline (1 cm) Axial Velocity/2 kg/s Air Flow. (The numbers denote central-jet flow rates of CO_2 in kg/hr.)

31

8 kg/hr that the off-centerline velocities remain negative near the centerbody face. Only in Figure 11 for 8 kg/hr central flow we see that the off-centerline velocity 1 cm from the centerline remains positive up to a z/d of about 0.25.

As in the case of the centerline velocity data, there is qualitative agreement in the trends for the off-centerline data between the predictions and measurements (see Figure 5 of Reference 14). Both show negative velocities for central flow rates less than 8 kg/hr. While the measurement shows that for 8 kg/hr flow the off-center velocity up to a z/d of 0.1 is negative, numerical calculation predicts small positive velocities. Furthermore, prediction gives a positive peak velocity of 11% annular inlet velocity occurring at a z/d of 0.16, whereas the measured peak of 30% occurs at a z/d of 0.3. As discussed in Paragraph 4.1.3.1, the off-centerline measurements also have not shown distinct velocity characteristics and rear stagnation points for different central flow rates. It is possible that this discrepancy stems from the fact that the reported experimental data represent the average values of several sets of measurements taken at different times. Conceivably, the data scatter and the associated uncertainty tend to mask small changes in the velocity characteristics and rear stagnation-point locations. Although the present predictions are restricted to isothermal flows, it is worth noting here that the measured data in combusting flow (see Figure 6 of Reference 14) do reveal, albeit slightly, the distinct profiles and rear stagnation points. It is presently unclear whether this arises because of the larger scatter and greater uncertainty associated with the combusting data.

4.1.3.3   Air as the Central-Jet Fluid

It was noted in Paragraph 3.2.1 that numerical calculations with air as the central-jet fluid were made with central-jet exit velocities that were the same as for CO_2 flow rates of 4, 6, and 8 kg/hr. These correspond respectively to air-flow rates of 2.6, 3.9, and 5.2 kg/hr. The predicted results with the air as the central fluid do not differ from those for CO_2 discussed in the previous paragraphs. Since this set of calculations was motivated by the experimental observation[14] that the linear dependence of the forward stagnation point on the central-jet exit velocity is independent of the central fluid used, we are concerned here only with the aspect relating to the centerline forward and rear stagnation points. Table 3 presents the z/d values of the forward and rear stagnation points for both CO_2 and air as the central fluid.

TABLE 3
CENTERLINE FORWARD AND REAR STAGNATION POINTS

Annular Mass Flow Rate	Central Jet Exit Velocity	CO$_2$ Flow Rate	Air Flow Rate	z/d			
				Forward Stagnation Point		Rear Stagnation Point	
kg/s	m/s	kg/hr	kg/hr	CO$_2$	Air	CO$_2$	Air
2	34.37	4	2.6	7.5×10^{-2}	6.33×10^{-2}	1.16	1.11
	51.54	6	3.9	1.45×10^{-1}	9.6×10^{-2}	1.22	1.11
	68.71	8	5.2	2.8×10^{-1}	1.63×10^{-1}	1.38	1.16

It is clear from the above that both the forward and rear stagnation points are predicted to lie closer to the centerbody face for air than for CO$_2$. Also, the disagreement becomes wider as the central-jet exit velocity increases, especially for the forward stagnation points. It has been already pointed out in paragraph 4.1.3.1 that the calculations do not predict the observed linear dependence of the forward stagnation point on the central-jet exit velocity. From the results in this paragraph, it would appear that the central-jet fluid does have a significant influence on the forward stagnation point. Thus, the data in Figure 8 of Reference 14 are not verified by numerical predictions at this time.

4.2 CENTRAL-JET DOMINANT FLOW REGIME

Following are the results of the predictive calculations when the central jet completely dominates the near-wake region behind the centerbody. The central flow rates considered are 4, 6, and 8 kg/hr of CO$_2$. Two sets of calculations are carried out. The first set employs an annular air mass flow rate of 0.07 kg/s, which is representative of the purge flows used in the experimental investigations to keep the seed material off the access windows. The second set has no annular flow and the central jet issues like a free jet, except for the presence of the centerbody and the outer confining duct. In either case of very small or zero annular flow, there is no recirculating flow present in the vicinity of the centerline. However, there are some distinct differences in the flowfield details between the two cases.

4.2.1 Very Small Annular Flow

The computed stream function contours for 8 kg/hr CO_2 flow rate are presented in Figure 13. The flow patterns for the two lower central flow rates are similar since for the purge annular flow under consideration, all three central-jet flows achieve complete penetration of the near-wake region by eliminating both the forward and rear stagnation points. Thus, the following discussion applies to the lower flow rates as well.

Figure 13 shows that the annular jet is being entrained by the central jet - a reverse situation of that seen in Figure 4 where small central flow is completely deflected by the reverse air flow along the centerline. A small vortex is set up close to the centerbody face and very near the annular jet. From the streamline contours it is clear that even a very small annular flow affects the spreading of the central jet. Beyond a z/d of 0.4, no significant spreading is observed; in fact, a small convergence of the central jet is seen, arising from the deflection of the annular jet toward the centerline.

The isovelocity contours for the mean axial velocity for 4 and 8 kg/hr CO_2 flow rates are seen respectively in Figures 14 and 15. Figure 15 confirms the occurrence of a minimum velocity region on the centerline between z/d values of 0.4 and 0.5. The centerline decay of axial velocity seen in Figure 16 identifies the local minimum in the axial velocity for all the three central flow rates. Figures 14 through 16 employ the annular inlet-plane velocity and centerbody diameter as the normalization quantities. When the fuel-jet velocity and the fuel-tube diameter (d_f) are used for normalization, the centerline velocity characteristics are more clearly depicted as seen in Figure 17. It is seen that only a small potential-core region (up to one diameter of fuel tube) occurs. Although an approximately linear decay (on the log-log plot) is seen, there is no monotonic velocity decay as would be expected in a free jet.[28] Instead, a local minimum develops between 8 and 15 z/d_f for all the three flow rates, after which the axial velocity increases again. Thus, it is seen that even very small annular flow has a pronounced effect on the central-jet development and velocity-decay characteristics.

4.2.2 Zero Annular Flow

In view of the nontrivial influence of the presence of the centerbody and annular flow noted in the previous paragraph, it is interesting to examine the flowfield of the central jet when the annular jet is completely absent. The results of central-jet flow rates of 4, 6, and 8 kg/hr are discussed in the following paragraphs.

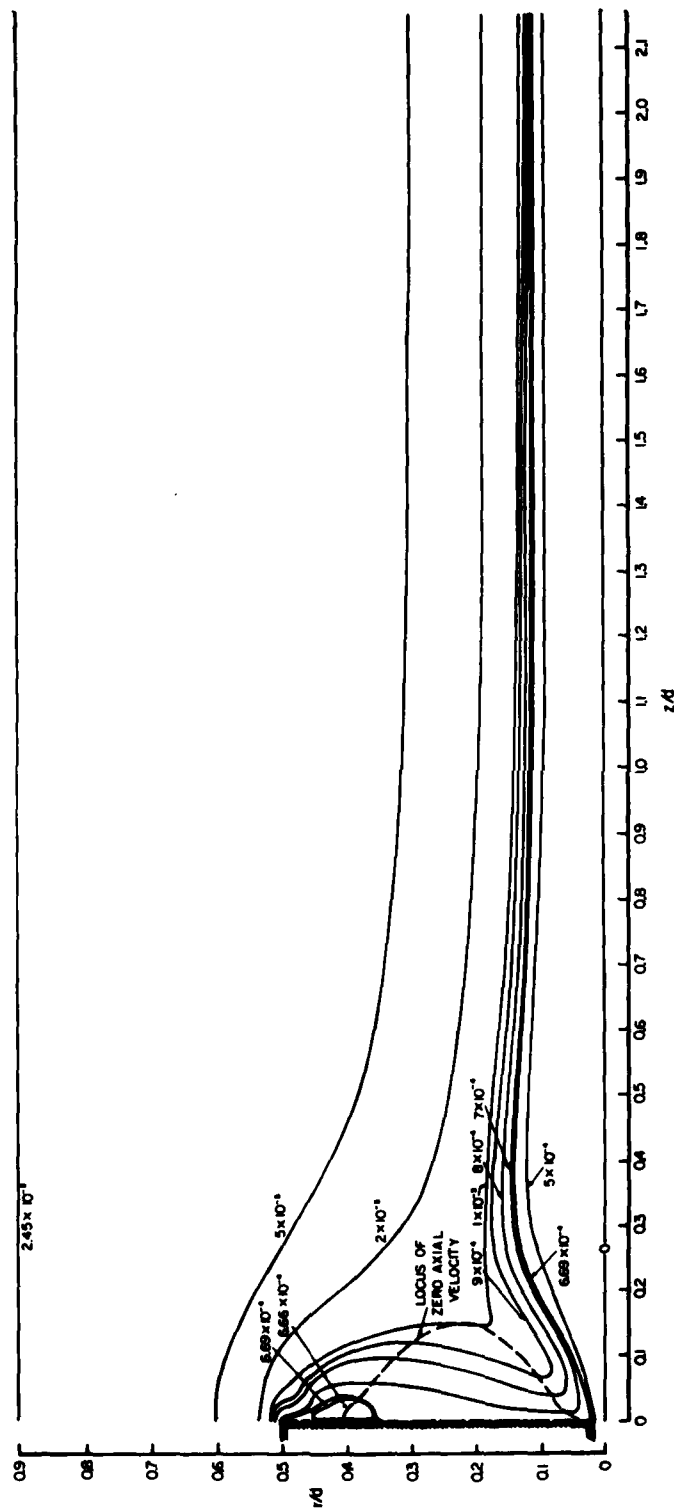Figure 13. Stream-Function Contours/0.07 kg/s Air Flow - 8 kg/hr CO_2 Flow.

35

Figure 14. Mean Axial Velocity Contours/0.07 kg/s Air Flow – 4 kg/hr CO_2 Flow. (Velocities are shown normalized with reference to the annulus inlet-plane velocity.)
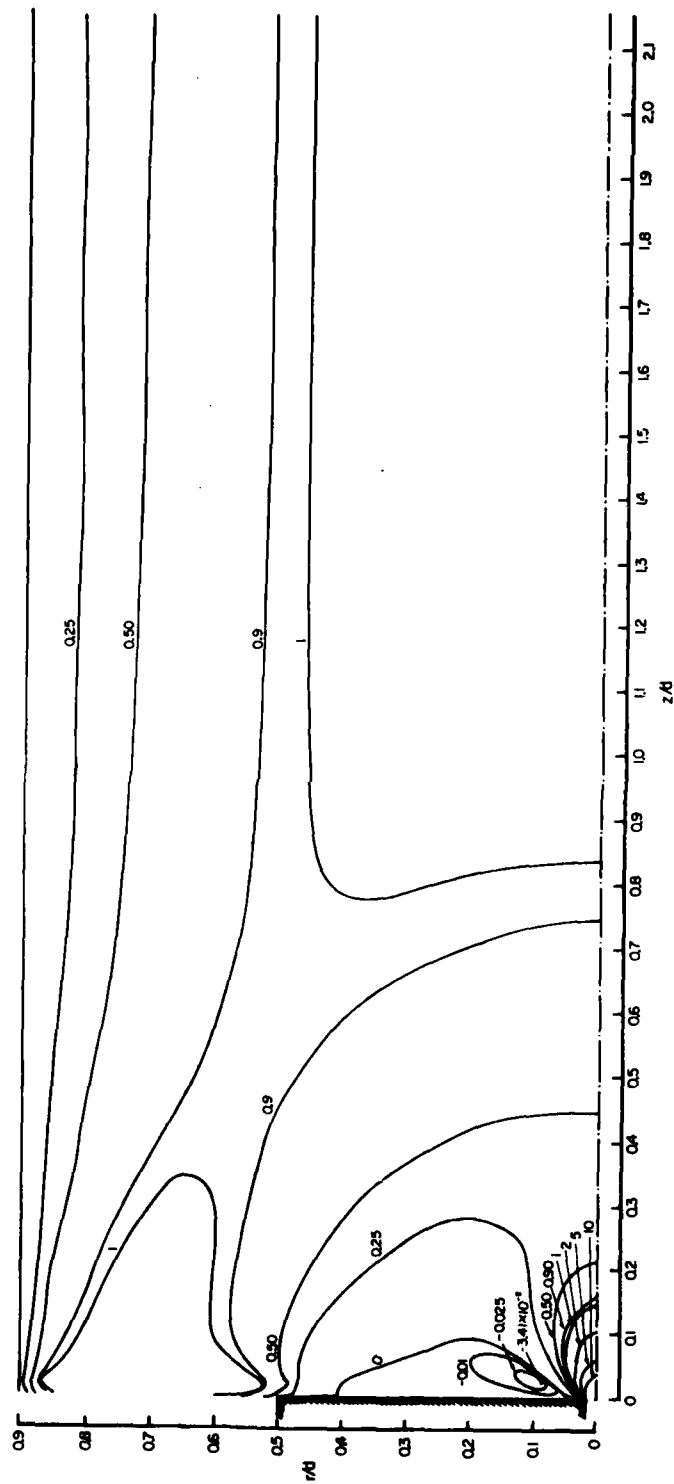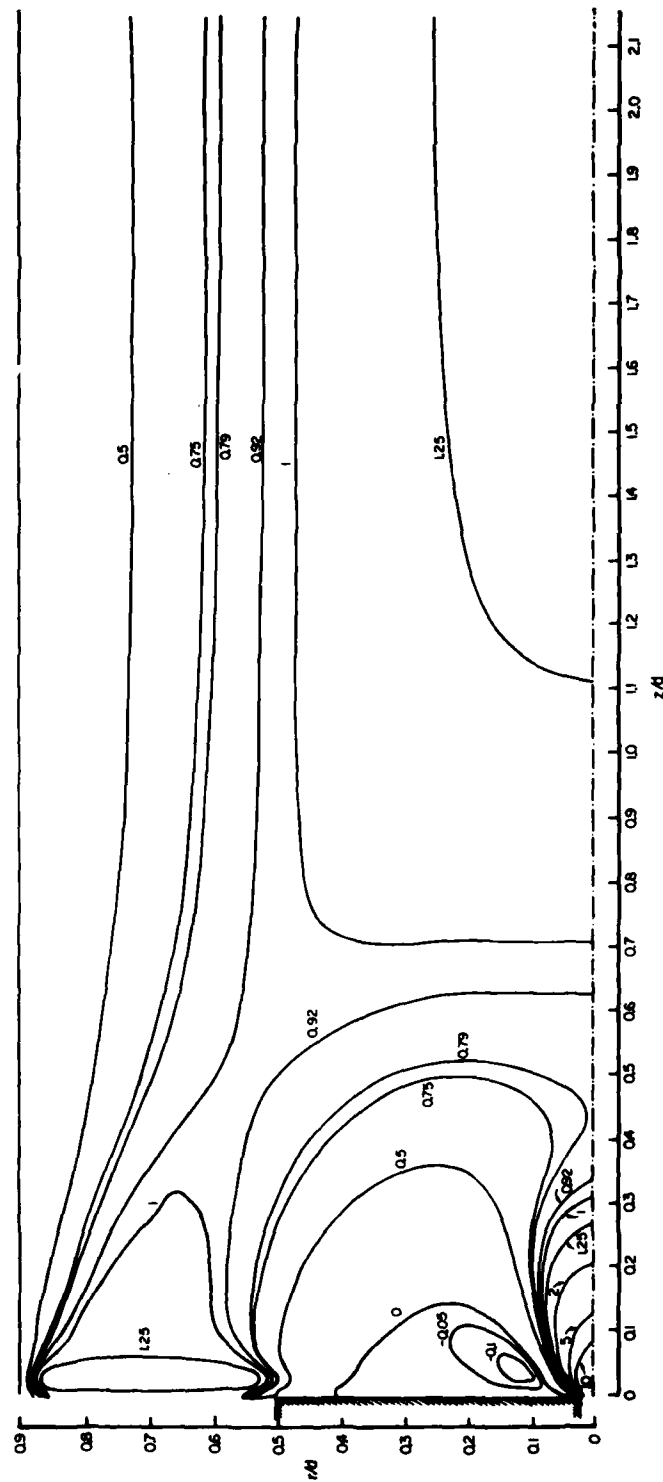
Figure 15. Mean Axial Velocity Contours/0.07 kg/s Air Flow - 8 kg/hr CO_2 Flow. (Velocities are shown normalized with reference to the annulus inlet-plane velocity.)
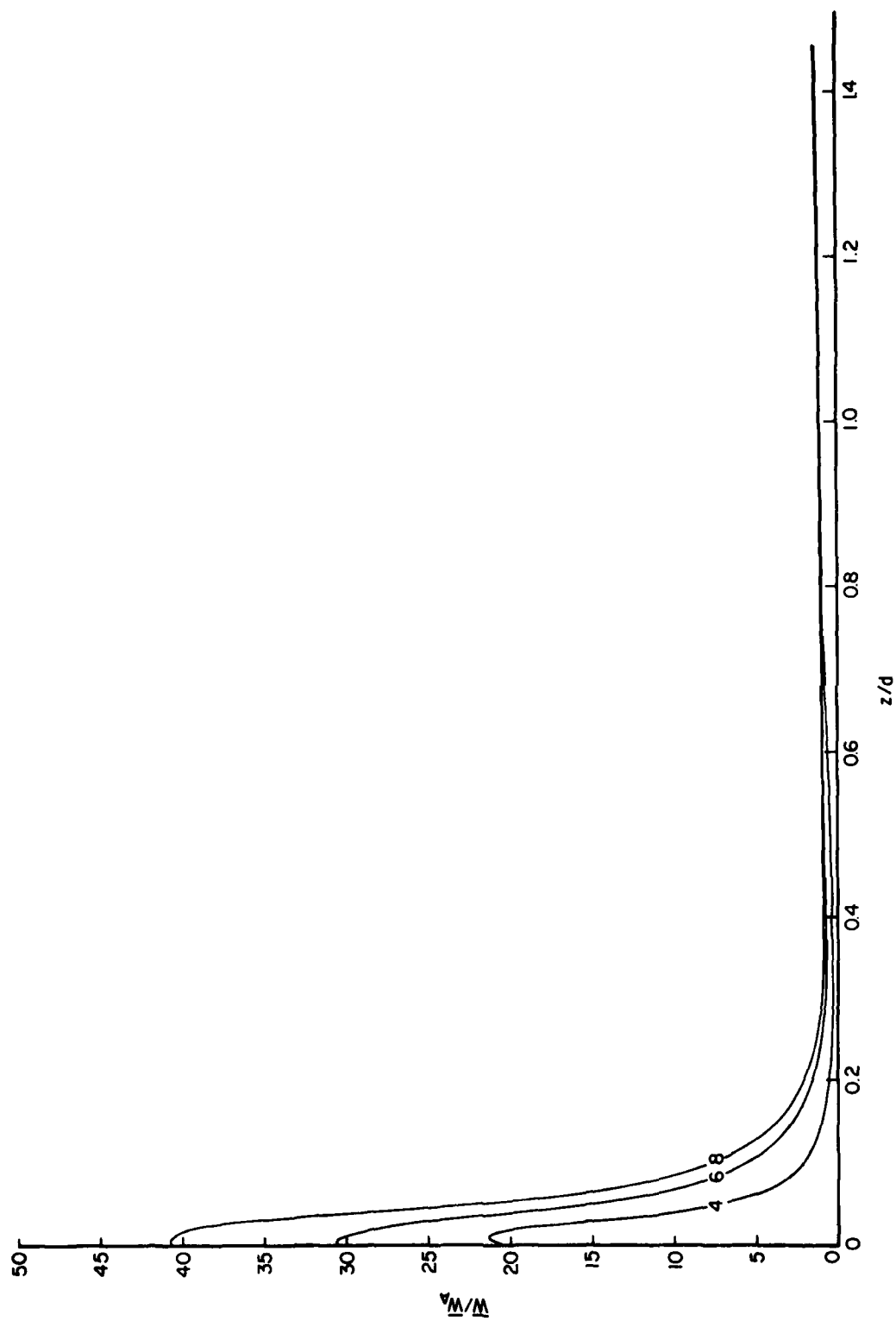
Figure 16. Axial Variation of Centerline Axial Velocity/0.07 kg/s Air Flow. (The numbers denote central-jet flow rates of CO_2 in kg/hr.)
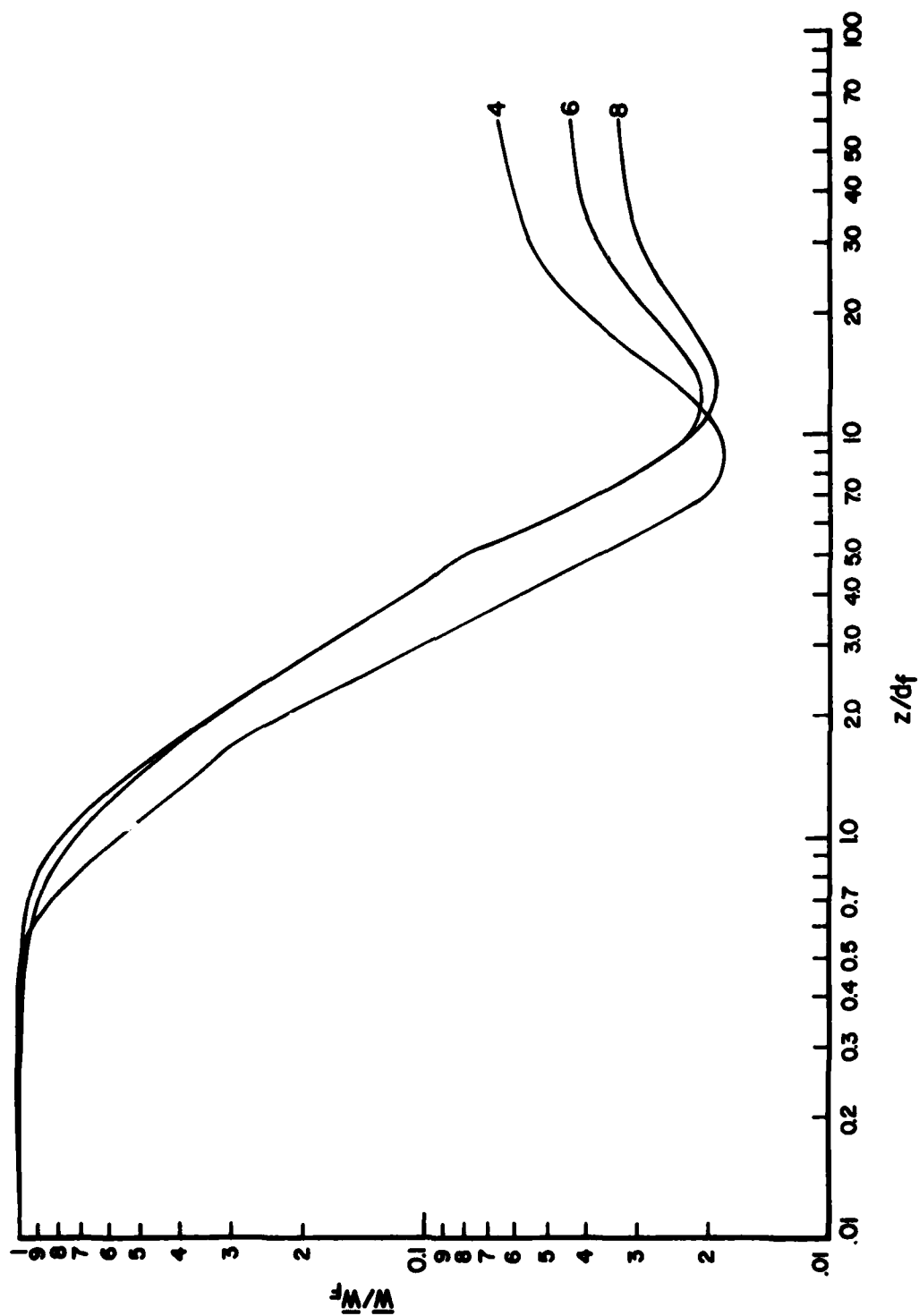
Figure 17. Axial Variation of Centerline Axial Velocity/0.07 kg/s Air Flow. (The numbers denote central-jet flow rates of CO_2 in kg/hr. Central-jet exit diameter and velocity are used for normalization.)

39

4.2.2.1 Stream-Function Fields

Figures 18 through 20 show the computed stream-function contours for the three central-jet flow rates considered. In the absence of the annular jet, the entrainment requirement of the central jet is satisfied by the setting up of a vortex between the centerbody face and the confining outer duct. It is a rather lazy recirculation zone that grows in axial extent as the central-jet flow rate increases. It is seen that the vortex center moves both axially and radially outward as the flow rate is increased. The reattachment point on the outer wall, determined by the intersection of the zero axial velocity line, also moves further downstream as the rate of central flow increases. The shift of the wall-reattachment point does not appear to be linear. It seems that this location would be a useful parameter for comparison of measurement and prediction. Figure 20 for the highest flow rate shows that the exit-plane boundary condition is satisfied to a lesser extent than for the two lower flow rates.

4.2.2.2 Axial Velocity Contours

The predicted isovelocity contours are seen in Figures 21 through 23. The velocity is normalized with respect to the central-jet exit velocity. We note that the velocities associated with the recirculation region are indeed small.

It seems from the isovelocity contours that initially the central jet is not significantly affected by the confining duct. Note that the initial development of a 4.8-mm diameter jet imbedded in a centerbody 140 mm in diameter differs little from the development of a jet issuing from an unbounded vertical wall. Perhaps, up to a z/d of 0.1, the central-jet development is not critically affected by the recirculation flow in the outer region. An examination of the centerline velocity characteristics in the next paragraph clarifies this point.

4.2.2.3 Axial Variation of Centerline Axial Velocity

The axial velocity profile on the centerline is shown in Figure 24. It is seen that the potential core exists for less than one diameter. The tendency for a log-log plot with slope of -1 is noticeable initially (less than 2, 6, and 9 diameters respectively for 4, 6, and 8 kg/hr CO_2 flow rates). Further downstream, the centerline velocity decays much faster than the 1/z power-law dependence characteristic of free turbulent circular jets.[28] Thus, the present predictions indicate that in the presence of the centerbody and confining duct the central jet does not behave like a free jet. It is not clear if this

40

Figure 18.   Stream-Function Contours at Zero Annular Flow/4 kg/hr CO_2 Flow.

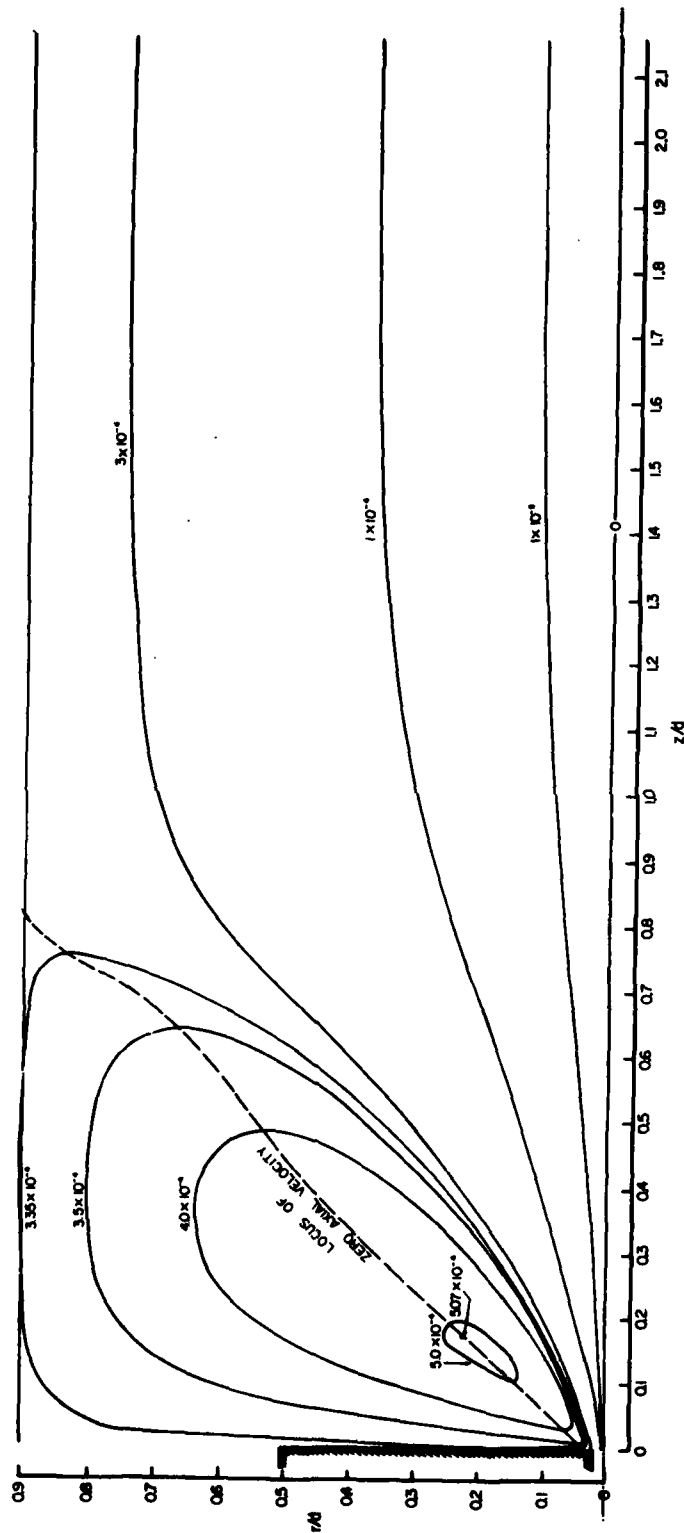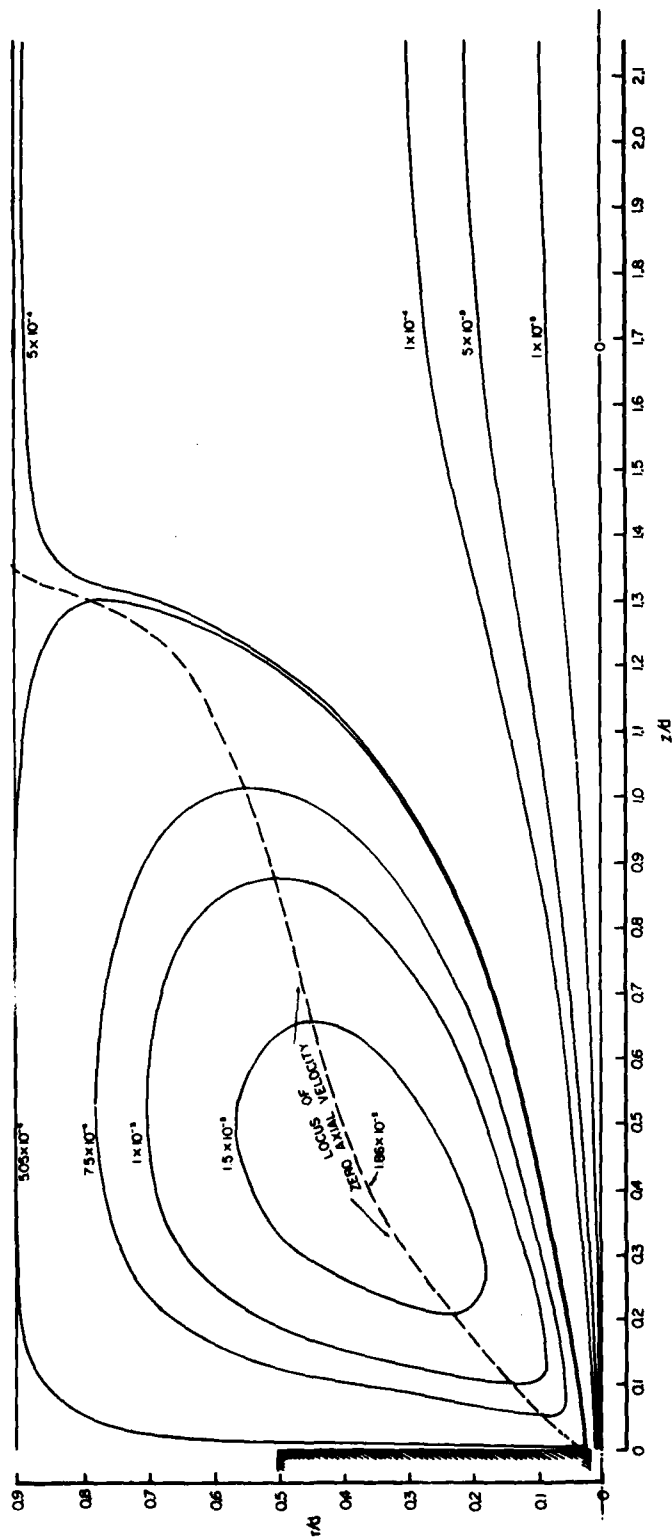Figure 19. Stream-Function Contours at Zero Annular Flow/6 kg/hr CO_2 Flow.

42
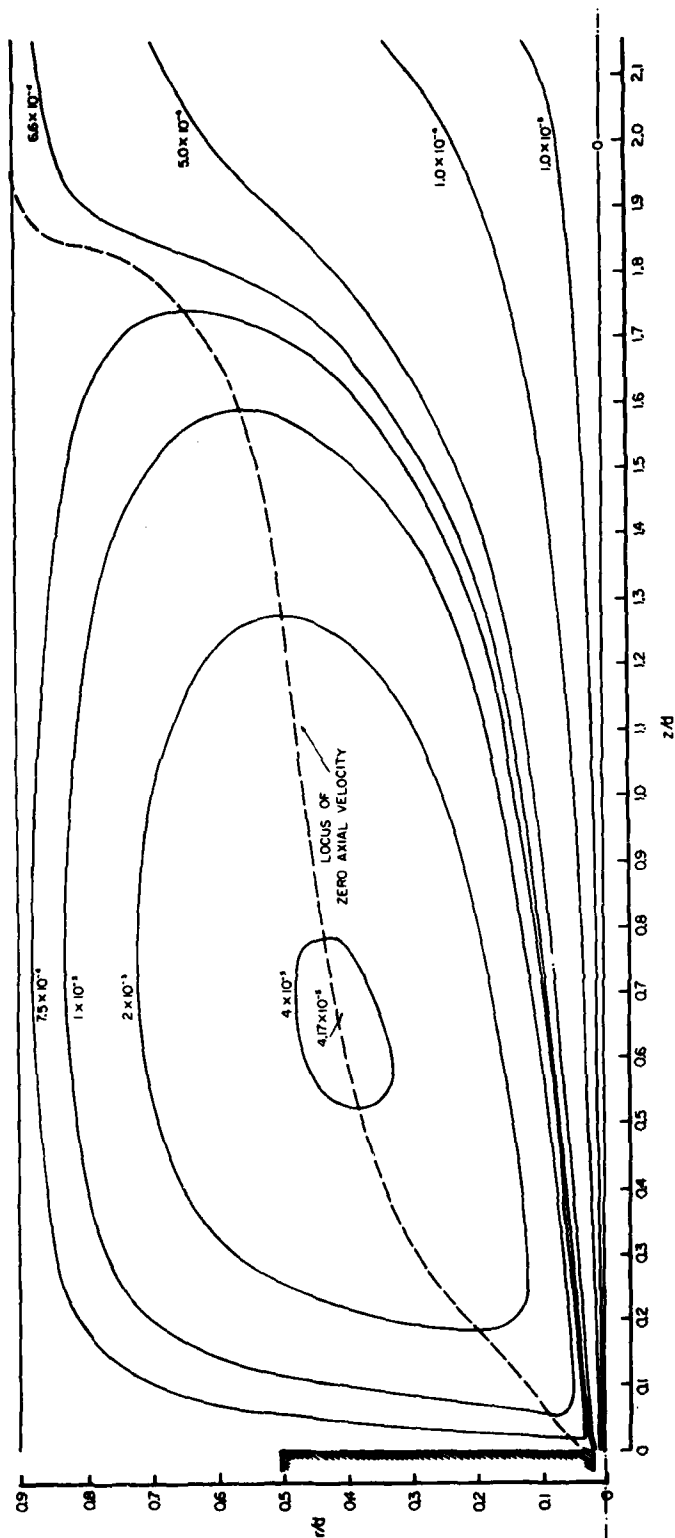
Figure 20. Stream-Function Contours at Zero Annular Flow/8 kg/hr CO_2 Flow.

43

Figure 21. Mean Axial Velocity Contours at Zero Annular Flow/4 kg/hr CO_2 Flow.

44
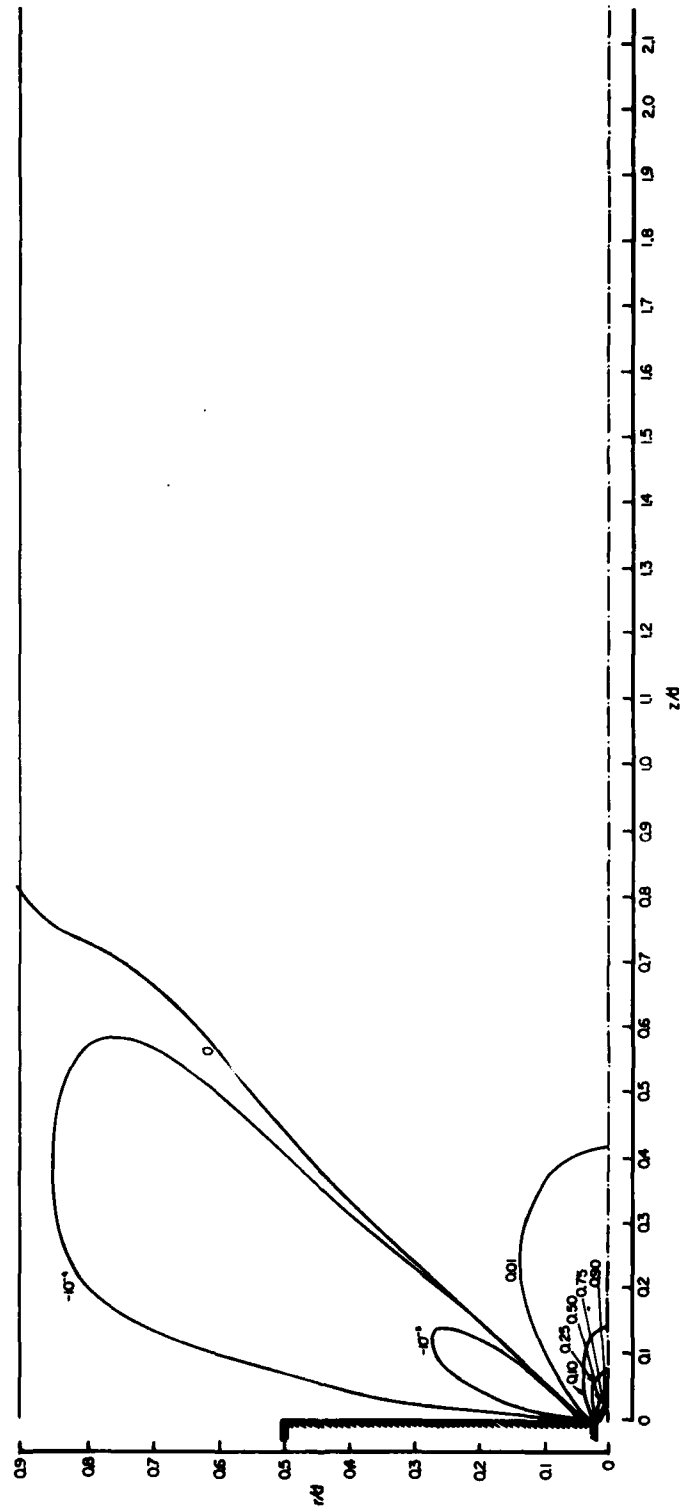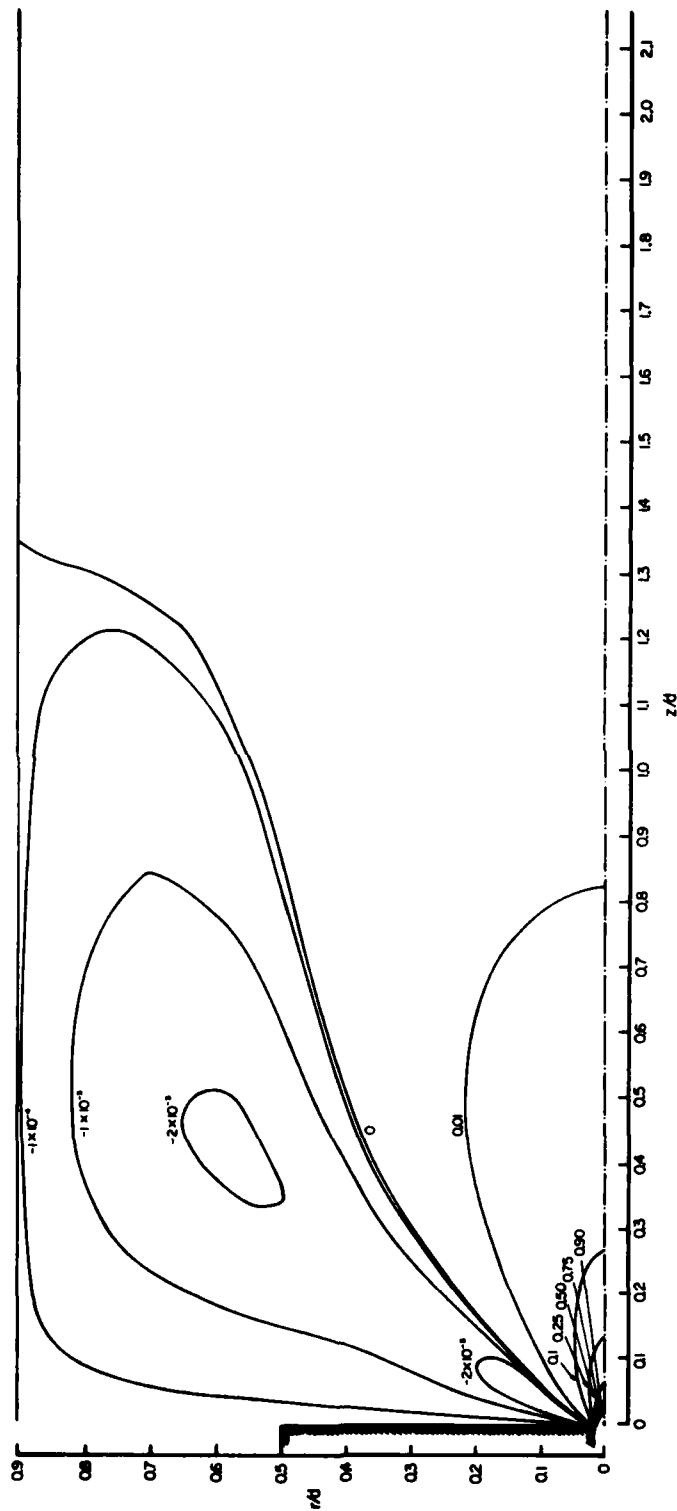
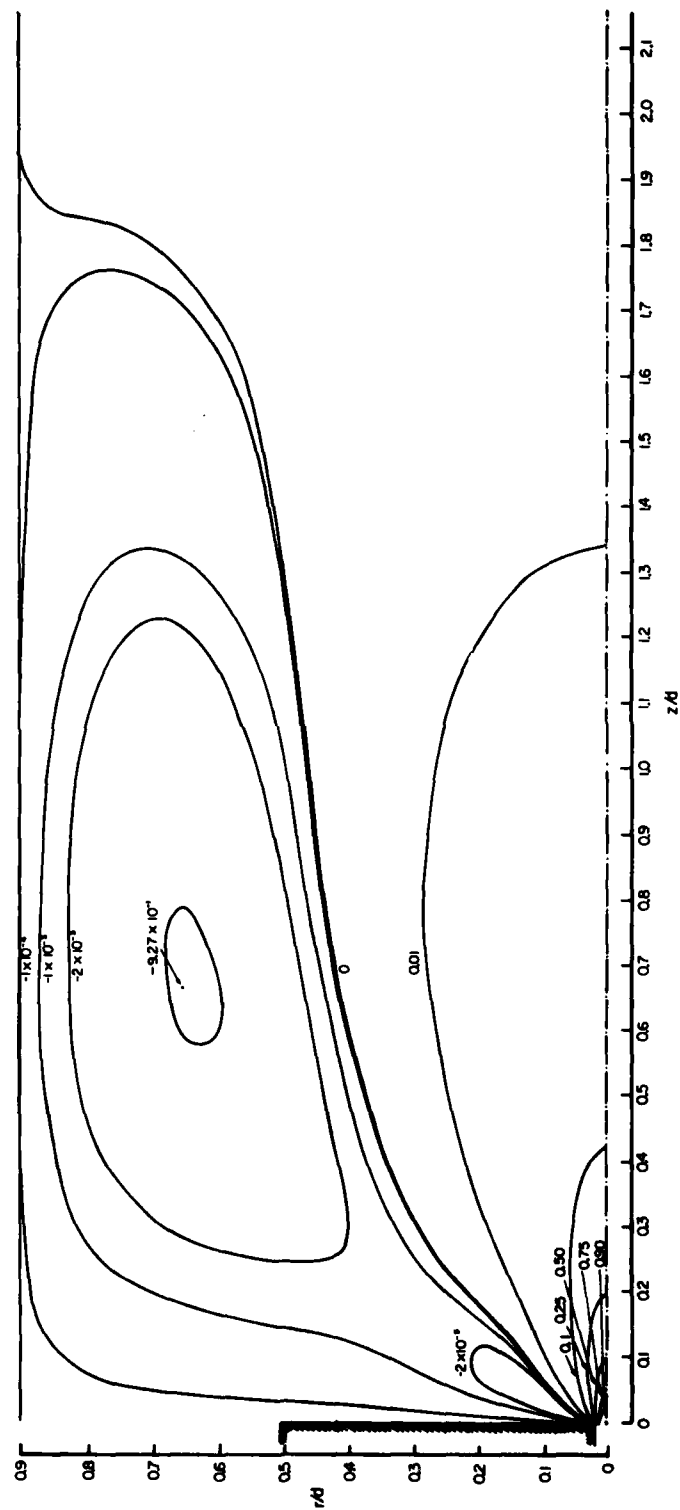Figure 22.   Mean Axial Velocity Contours at Zero Annular Flow/6 kg/hr CO_2 Flow.

45

Figure 23. Mean Axial Velocity Contours at Zero Annular Flow/8 kg/hr CO_2 Flow.
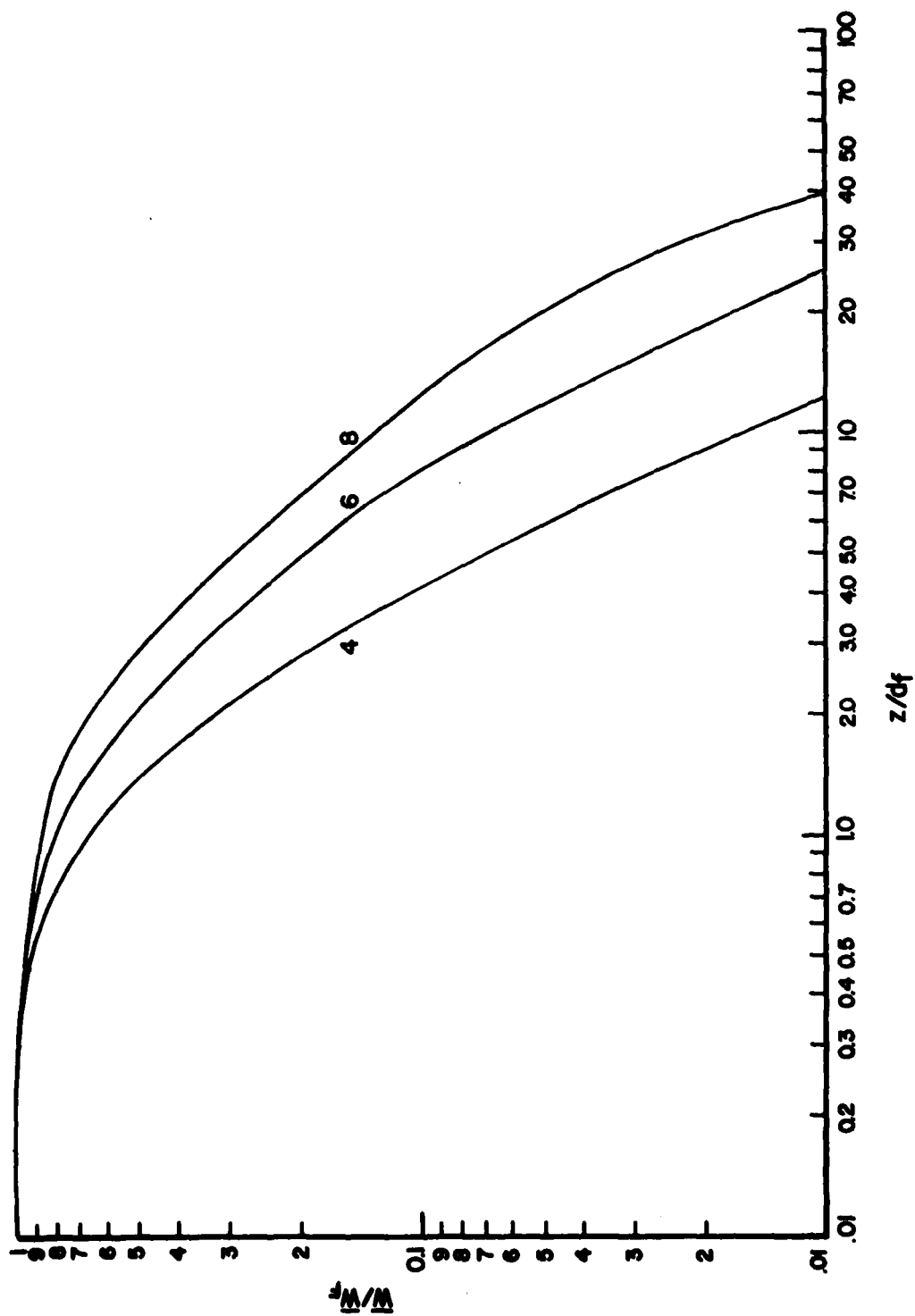
Figure 24. Axial Variation of Centerline Axial Velocity at Zero Annular Flow. (The numbers denote central-jet flow rates of CO_2 in kg/hr. Central-jet exit diameter and velocity are used for normalization.)

47

observation is real or is attributable to the failure of the numerical model (using a constant eddy-viscosity formulation) to predict correctly the velocity-decay characteristics.

4.3 PREDICTION OF CONCENTRATION FIELDS

The numerical computations outlined in Section III include the predictions of mass fractions of CO_2 in the flowfield. The predicted results discussed in the following paragraphs are based on the assumption of unity effective Schmidt number and thus on the constant eddy viscosity model.

4.3.1 Mass-Fraction Contours in Annular-Flow Dominant Regime

The local CO_2 mass-fraction field predicted for the annular air flow of 2 kg/s and central CO_2 flow rates of 4, 6, and 8 kg/hr is seen respectively in Figure 25 (a), (b), and (c). The mass-function contour corresponding to the CO_2 mass fraction of 0.06 is also included since it is the stoichiometric value of fuel mass fraction for propane/air combustion. The mass-fraction contours in (a) and (b) show that the radial extent is much more than the axial extent - a result directly caused by the radially outward deflection of the CO_2 jet by the reverse-flow air. Compared to the 4 kg/hr flow rate, the 6 kg/hr flow rate in (b) merely indicates a greater spreading of CO_2 in the axial direction. In (c), one notices a much larger penetration in the outer shear layer, especially for the 0.06 contour. While a direct correspondence with the combusting flow is not necessarily indicated, the mass-fraction contour for 0.06 does show the region most likely to experience combustion reactions.

4.3.2 Centerline CO_2 Mass Fractions

The axial variation of the CO_2 mass fraction on the centerline is seen in Figure 26. Here, the cases of both annular-jet dominant regime and the central-jet dominant regime are shown. For the latter case, the results of very small annular flow and of zero annular flow are presented. The general trends of the predicted results are essentially correct. For the annular-flow dominant condition, the centerline mass fraction decays rapidly to small values and then equally rapidly approaches uniform values. For the isothermal flows under consideration, the changes in mass fraction arise only from convective and diffusive fluxes. On the centerline the radial component of velocity is zero and the convection is strictly in the axial direction. Because of symmetry requirements, the radial gradients also vanish on the centerline. Thus, the diffusive flux is only in the axial

48
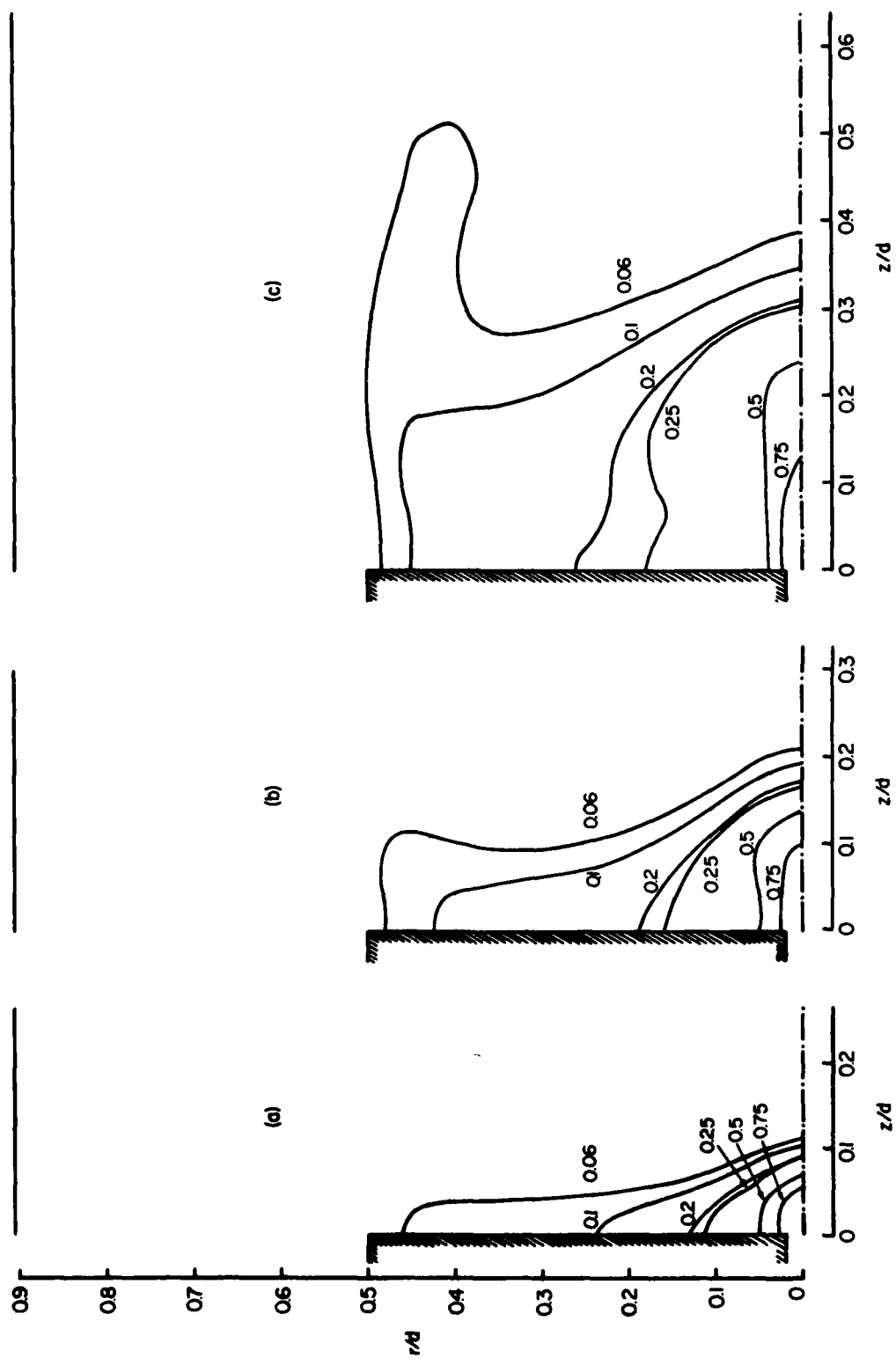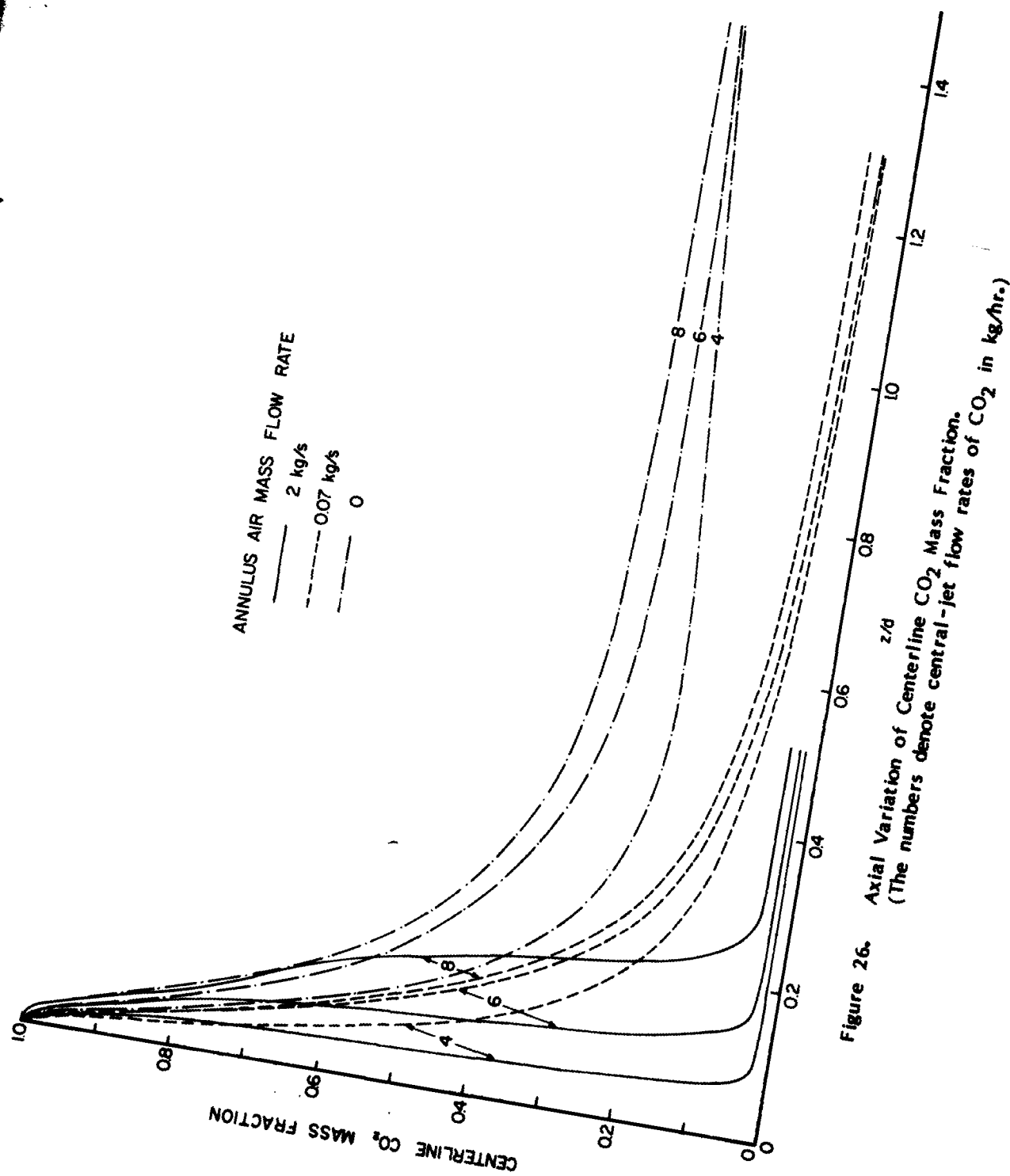
Figure 25. Local CO_2 Mass-Fraction Contours/2 kg/s Air Flow. (a) 4 kg/hr CO_2 Flow (b) 6 kg/hr CO_2 Flow (c) 8 kg/hr CO_2 Flow.

49

Figure 26. Axial Variation of Centerline CO_2 Mass Fraction.
(The numbers denote central-jet flow rates of CO_2 in kg/hr.)

50

direction. Since the axial velocity decreases rapidly and then vanishes at the forward stagnation point, it is reasonable to expect the rapid decay of CO_2 mass fraction. (Diffusion only tends to enhance the decay.) Beyond the forward stagnation point, the axial velocity is negative. Here the convection and diffusion tend to oppose each other. The CO_2 mass fraction at a point in question tends to increase by convective flux and tends to decrease by diffusive flux. This results in a rapid approach to a nearly uniform condition after the forward stagnation point. Thus, it is clear that the turning of the centerline profile occurs in the vicinity of the forward stagnation point. A confirmation of this observation can be obtained by comparing Figures 26 and 5. The points of intersection obtained by extrapolating the portions of the profiles that denote the rapid decay and approach to uniformization in Figure 26 fall very close to the forward stagnation points in Figure 5. Recent concentration measurements[29] by probe sampling and their correlation with earlier velocity measurements[14] tend to support this viewpoint.

The centerline profiles for very small annular flow show a more gradual decay and the asymptotic uniform values are higher than the previous case, as could be expected. When there is no annular flow, the concentration decay is the slowest and the uniform values further downstream are the highest. These observations have the right qualitative trends. While the centerline profiles for 6 and 8 kg/hr CO_2 flow rates with no annular air show the expected monotonic decay, the profile for 4 kg/hr shows a local minimum. It is unclear at present if this occurs in reality.

51

SECTION V
CONCLUDING REMARKS

This section outlines the main conclusions emerging from the work, followed by recommendations offered in the light of these conclusions.

5.1 CONCLUSIONS

a. The isothermal modeling under a constant eddy viscosity model has been successful in providing reasonably correct qualitative predictions of centerbody combustor flowfields.

b. The numerical predictions have generally confirmed the heuristic flowfield descriptions suggested earlier for delineating different flowfield regimes.

c. The predicted results of the flowfields when the annular flow dominates the near-wake flow show overall trends that are in conformity with the experimental observations.

d. The z/d values for the centerline forward stagnation points are calculated to be 0.08 and 0.28 respectively for central CO_2 flow rates of 4 and 8 kg/hr (at an annular air flow rate of 2 kg/s), whereas the laser Doppler anemometry measurements report values of 0.3 and 0.5. Thus, present numerical results underpredict the forward stagnation points on the centerline and do not show the observed linear dependence with central-jet exit velocity.

e. The z/d values for the centerline rear stagnation points are calculated to be 1.15 and 1.38 respectively for central CO_2 flow rates of 0 and 8 kg/hr (at an annular air flow rate of 2 kg/s), whereas the measured value is 0.9 and remains unaffected by the change in central flow rate.

f. The predictions of both the radial and axial coordinates of the negative vortex in the annular-jet dominant regime show physically consistent behavior and agree with the results of recent annular-jet measurements.

g. For the annular-jet dominant regime (2 kg/s annular air flow), the computed axial velocity profiles in the reverse-flow region for the four central CO_2 flow rates considered remain distinct with different values of centerline negative peak axial velocity. The measured velocity profiles, on the other hand, merge beyond the negative peak location for the zero central flow. For the zero central flow, the measured negative maximum of 42 percent of the annular inlet-plane velocity is found to occur at a z/d of 0.4, while the computed maximum of 53 percent occurs at a z/d of 0.35. In the computations, the largest peak negative velocity of 62 percent at a z/d of 0.38 occurs for 4 kg/hr CO_2 flow rate.

h. In flow situations where the annular jet dominates the near-wake flowfield, the predicted centerline decay of CO_2 mass fraction shows fair agreement with the experimental trends. Also, the changeover of the profile from a rapid decay to a nearly uniform value occurs very close to the forward stagnation point.

i. Predictions do not support the experimental observation where the location of the forward stagnation point on the centerline depends only on the central-jet exit velocity and not on the central-jet fluid. In other words, for the same exit velocity the calculated centerline locations of forward stagnation point for CO_2 and air are different.

j. Present numerical computations fail to converge to acceptable solutions for large central flow rates. This occurs irrespective of the annular flow rate.

k. Predictions in the flow regimes where the central jet dominates the flowfield show differences between the case where the annular flow is very small and the case where the annular flow is absent.

l. When even a small annular air flow is present, the centerline decay of axial velocity is not monotonic and a local minimum occurs.

m. With annular flow absent, the centerline decay of axial velocity is monotonic, but the decay appears to be faster than that of the free jet.

5.2 RECOMMENDATIONS

The present study offers the following recommendations for further activity.

a. It is necessary to have accurate inlet velocity profiles. Both axial and radial components of the mean velocity must be given. It is also necessary to know the level of inlet turbulence.

b. Both axial and radial components of the mean velocity as well as the fluctuations should be measured near the salient points of the flowfield (vortex centers, stagnation points etc., for example).

c. The axial variation of both centerline and off-centerline (along vortex centers) measurements of the variables must be made.

d. The radial profiling of mean velocities, normal and shear stresses, and mean concentrations should be done at the points in the flowfield mentioned in b above.

e.   The accuracy of laser Doppler anemometry measurements must be improved so that the dependence of the centerline variation of the axial velocity and of the location of the rear stagnation point on the central-jet flow rate could be determined.

f.   The numerical modeling needs significant improvement on several aspects. The eddy-viscosity approach appears to have considerable difficulty in predicting the central-jet development and velocity-decay characteristics. Turbulence models involving the direct solution of the equations for Reynolds stresses might be worthwhile. The applicability of time-averaged equations in situations like that of the centerbody combustor is questionable but an alternative formulation is not available at present.

REFERENCES

1. Development of Combustor Flow Analysis, Part I: Theoretical Studies; Part II: Experimental Studies, Air Force Aero Propulsion Laboratory, Air Force Systems Command, Wright-Patterson Air Force Base, Ohio, AFAPL-TR-73-96, January 1974.

2. Development of a Three-Dimensional Combustor Flow Analysis, Vol. I: Theoretical Studies; Vol. II: Theoretical Studies; Vol. III: User's Manual for the MINT Combustor Code, Air Force Aero Propulsion Laboratory, Air Force Systems Command, Wright-Patterson Air Force Base, Ohio, AFAPL-TR-75-59, October 1976.

3. M. A. Serag-Eldin and D. B. Spalding, "Computation of Three-Dimensional Gas Turbine Combustion Chamber Flows," ASME Paper 78-GT-142, presented at Gas Turbine Conference and Products Show, London, England, 1978.

4. Combustor Design Criteria Validation, Vol. I: Element Tests and Model Validation; Vol. II: Development Testing of Two Full-Scale Annular Gas Turbine Combustors; Vol. III: User's Manual, Applied Technology Laboratory, U. S. Army Research and Technology Laboratories (AVRADCOM), Fort Eustis, Virginia, USAFTL-TR-78-55 A, B, C, March 1979.

5. J. Odgers, "Combustion Modeling Within Gas Turbine Engines, Some Applications and Limitations," AGARD Conference Preprint No. 175, Combustion Modelling, AGARD, 1979, pp. 25-1-25-13.

6. J. Swithenbank, A. Turan, P. G. Felton, and D. B. Spalding, "Fundamental Modelling of Mixing, Evaporation and Kinetics in Gas Turbine Combustors," AGARD Conference Preprint No. 275, Combustion Modelling, AGARD 1979, pp 2-1-2-18.

7. D. G. Lilley, "Flowfield Modeling in Practical Combustor: A Review," Journal of Energy, Vol. 3, No. 4, July-August 1979, pp. 193-210.

8. Summary Report: D. O. D. Colloquium on Gas Turbine Combustor Modeling, Project SQUID Technical Report PU-RI 79, Published for ONR by Purdue University, November 1979.

9. L. Krishnamurthy, Discussion and Verification of FREP Code, Report M/WPAFB/COMB/78-1, School of Mechanical Engineering, Purdue University, West Lafayette, Indiana, July 1978.

10. L. Krishnamurthy, "Numerical Modeling of a Flowfield in a Dump Combustor," 5th Annual Minisymposium on Aerospace Science and Technology, Wright-Patterson Air Force Base, Ohio, March 21, 1979.

11. L. Krishnamurthy, Combustor Modeling Assessment Studies, Report UDR-TR-79-111, University of Dayton Research Institute, Dayton, Ohio, December 1979.

12. S. A. Syed and G. J. Sturgess, "Validation Studies of Turbulence and Combustion Models for Aircraft Gas Turbine Combustors," paper to be presented to ASME Winter Annual Meeting, Chicago, November 1980.

REFERENCES (Continued)

13. W. M. Roquemore, R. P. Bradley, J. S. Stutrud, C. M. Reeves, and
    L. Krishnamurthy, "Preliminary Evaluation of a Combustor for Use in Modeling and
    Diagnostics Development," ASME-80-GT-93, Twenty-fifth Annual International Gas
    Turbine Conference, The American Society of Mechanical Engineers, New Orleans,
    Louisiana, March 1980.

14. A. J. Lightman, R. D. Richmond, P. D. Magill, L. Krishnamurthy, W. M. Roquemore,
    R. P. Bradley, J. S. Stutrud, and C. M. Reeves, "Velocity Measurements in a
    Bluff-Body Diffusion Flame," AIAA-80-1544, AIAA 15th Thermophysics Conference,
    Snowmass, Colorado, July 1980.

15. N. A. Chigier and J. M. Beer, "The Flow Region Near the Nozzle in Double
    Concentric Jets," Journal of Basic Engineering, December 1964, pp. 797-804.

16. D. F. G. Durao and J. H. Whitelaw, "Velocity Characteristics of Disc-Stabilized
    Diffusion and Premixed Flames," AIAA Paper 76-34, January 1976.

17. M. M. M. Abou Ellail, A. D. Gosman, F. C. Lockwood, and I. E. A. Megahed,
    "Description and Validation of a Three-Dimensional Procedure for Combustion
    Chamber Flows," AIAA 77-138, AIAA 15th Aerospace Sciences Meeting, Los
    Angeles, California, January 1977.

18. P. Hutchinson, E. E. Khalil, and J. H. Whitelaw, "Measurement and Calculation of
    Furnace-Flow Properties," Journal of Energy, Vol 1, July-August 1977,
    pp. 212-219.

19. B. Lenze, "The Influence of Recirculation on Enclosed Turbulent Jet Diffusion
    Flames," 1977 Spring Technical Meeting, Central States Section/The Combustion
    Institute, Cleveland, Ohio, March 1977.

20. D. G. Elliman, D. E. Fussey, and M. Hay, "Predictions and Measurements of a
    Turbulent, Axisymmetric Ducted Diffusion Flame," International Journal of Heat
    and Mass Transfer, Vol. 21, 1978, pp. 1393-1402.

21. N. W. M. Ko and W. T. Chan, "Similarity in the Initial Region of Annular Jets;
    Three Configurations," Journal of Fluid Mechanics, Vol. 84, Part 4, 1978,
    pp. 641-656.

22. W. T. Chan and N. W. M. Ko, "Coherent Structures in the Outer Mixing Region of
    Annular Jets," Journal of Fluid Mechanics, Vol. 89, Part 3, 1978, pp. 515-533.

23. N. W. M. Ko and W. T. Chan, "The Inner Regions of Annular Jets," Journal of
    Fluid Mechanics, Vol 93, Part 3, 1979, pp. 549-584.

24. D. W. Peaceman and H. H. Rachford, Jr., "The Numerical Solution of Parabolic
    and Elliptic Differential Equations," Journal of the Society of Industrial and
    Applied Mathematics, Vol. 3, No. 1, 1955, pp. 28-41.

REFERENCES (Continued)

25. D. F. G. Durao and J. H. Whitelaw, "Velocity Characteristics of the Flow in the Near Wake of a Disk," *Journal of Fluid Mechanics*, Vol. 85, Pt. 1, 1979. pp. 185-207.

26. S. B. Pope and J. H. Whitelaw, "The Calculation of Near-Wake Flows," *Journal of Fluid Mechanics*, Vol. 73, Part 1, 1976, pp. 9-32.

27. A. D. Gosman, W. M. Pun, A. K. Runchal, D. B. Spalding, and M. Wolfshtein, *Heat and Mass Transfer in Recirculating Flows*, Academic Press, London, 1969, p. 212.

28. P. T. Harsha, "Free Turbulent Mixing: A Critical Evaluation of Theory and Experiment," AEDC-TR-71-36, 1971.

29. W. M. Roquemore, Private Communication, 1980.

DATE
ILME